Physics – Uspekhi **55** (8) 773 – 789 (2012)

INSTRUMENTS AND METHODS OF INVESTIGATION PACS numbers: **07.35.+k**, 42.70.Ce, **62.50.–p**, 91.60.Fe, **96.12.–a**

Shock compression of porous metals and silicates

A B Medvedev, R F Trunin

DOI: 10.3367/UFNe.0182.201208b.0829

Contents

Abstract. This paper reviews the results of experimental research on shock-compressed porous metals conducted in laboratory conditions and underground nuclear explosion environments. The general properties of shock adiabats are discussed. A rather simple wide-range equation of state is applied to describe the totality of test data. Porous metals and silicates are comparatively studied for, and found to qualitatively differ in, their behavior over a wide pressure range (tens of GPa). A possible explanation for the nonstandard behavior of silicates is that the Grüneisen coefficient in these states of matter can assume negative values at elevated pressures and temperatures. A similar anomaly is hypothesized to account for the superadiabatic density growth in the upper mantle of Earth.

1. Introduction

Equations of state (EOSs) are of great importance in the solutions to various scientific and technical problems. In particular, EOSs of metals are widely used in designing high-energy facilities of different types, and EOSs of silicates are of significance for geophysics and planetology.

A B Medvedev Russian Federal Nuclear Center — The All-Russian Research Institute of Experimental Physics,
prosp. Mira 37, 607190 Sarov, Nizhny Novgorod region, Russian Federation
Tel. +7 (83130) 2 20 31. Fax +7 (83130) 2 03 20
E-mail: postmaster@ifv.vniief.ru
R F Trunin Sarov Institute of Physics and Technology — Branch of the National Research Nuclear University MEPhI,
ul. Dukhova 6, 607186 Sarov, Nizhny Novgorod region, Russian Federation
Tel. +7 (83130) 7 68 63. Fax +7 (83130) 3 48 09
E-mail: rector@sarfti.ru

Received 8 August 2011, revised 20 December 2011
Uspekhi Fizicheskikh Nauk **182** (8) 829 – 846 (2012)
DOI: 10.3367/UFNr.0182.201208b.0829
Translated by E N Ragozin; edited by A Radzig

One of the main sources (and in many cases the sole one) of information about the thermodynamic properties of substances at the high pressure P, density ρ, and internal energy E is experimental shock compression data. These data are substantially used in determining the parameters of semiempirical model EOSs and serve as test data for verifying *a priori* theoretical models at the highest achieved parameter values.

In shock wave research, primary emphasis is placed on the study of shock Hugoniots which characterize an initially continuous substance with an initial density ρ_0 corresponding to normal conditions: $P_0 = 1$ atm, $T_0 = 298$ K (principal Hugoniots). These adiabats were determined for a large number of substances over a broad range of compression degrees $\sigma = \rho/\rho_0 > 1$ (as a rule, up to $\sigma \approx 2-3$ and sometimes higher). The materials of these investigations are the subject of numerous papers and have repeatedly been published in a generalized form [1–7]. Detailed experimental information is given in reference books [8–10].

In the study of material's EOSs, use is also made of the methods for shock compression of porous samples, double shock compression, isentropic unloading, etc. The phase diagram domains attainable by these methods are qualitatively depicted in Fig. 1 in (P, V) coordinates ($V = 1/\rho$ is the specific volume) by the example of a metal.

Experiments on the shock compression of porous samples characterized by a lowered initial density permit covering the range of states with higher values of E and temperature T than those realized in the principal Hugoniot. The values of σ also differ significantly. The resultant data possibly pertain to the domain of states corresponding to $\sigma < 1$ (in this case, the degree of substance expansion $1/\sigma > 1$). This information is fundamentally important in the construction of EOS models.

A rather large number of papers are concerned with investigations of substance properties by the shock compression of initially porous samples. However, the resultant data are insufficiently amply covered in the papers cited above. Eliminating this shortcoming is one of the goals of our review.

In this paper we set out the results of investigations into the shock compressibility of porous metals, the main body of

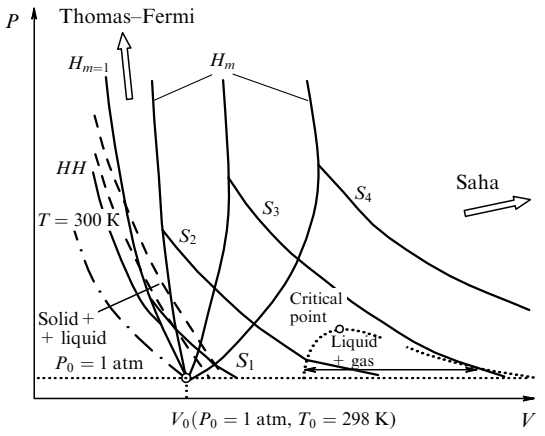

Figure 1. Schematic representation of the phase diagram of metals: $H_{m=1}$ – principal shock Hugoniot; H_m — Hugoniots of an initially porous substance; HH — double compression Hugoniot, with the dashed–dotted line standing for the $T = 300$ K isotherm; $S_1 - S_4$ – isentropes of expansion from shock-compressed states. The dashed curves bound the domain in which the substance is a mixture of solid and liquid phases.

which was performed in Russia. The characteristic properties of the heated metals revealed in these experiments are discussed. The totality of experimental data is described, proceeding from a relatively simple wide-range model EOS.

Silicates are discussed along with metals. One of the objectives of the combined consideration of these two substance types is to demonstrate the qualitative difference between the behavior of silicates and the normal behavior of metals in a wide pressure range (on the order of several dozen GPa). Our thermodynamic analysis of the shock compression data for continuous and porous samples suggests that the unconventional behavior of silicates may be attributed to the realization of substance states characterized by negative ('anomalous') values of the Grüneisen and thermal expansion coefficients. We describe the data of experiments on fused and porous silicon proceeding from a model EOS describing this anomaly. A manifestation of an anomaly of this kind in the upper mantle of Earth is hypothesized in Section 7.

2. Method of investigation for the shock compression of porous substances

The study of substance compressibility under shock wave action relies on recording two kinematic characteristics of a stationary shock wave propagating through a material with fixed initial parameters — a shock wave velocity D, and a particle velocity U behind the wave front. The set of measured D and U values for different shock intensities defines the experimental dependence $D(U)$, which corresponds to a substance with initial density ρ_{00}, pressure P_{00}, and internal energy E_{00}. Under shock compression, the parameters are related by mass, momentum, and energy conservation equations:

$$\rho = \rho_{00}\,\frac{D}{D-U}\,, \tag{1}$$

$$P = P_{00} + \rho_{00} D U\,, \tag{2}$$

$$E = E_{00} + \frac{(P+P_{00})(V-V_{00})}{2}\,, \tag{3}$$

where $V_{00} = 1/\rho_{00}$. Proceeding from Eqns (1)–(3) and invoking the experimental $D(U)$ dependence, it is possible to calculate in the hydrodynamic approximation (neglecting the relatively weak material strength, which is ordinarily on the order of several GPa) the shock Hugoniot in any other variables, in particular P, σ or P, V. The case where $\rho_{00} = \rho_0$, $P_{00} = P_0 = 1$ atm, $E_{00} = E_0 = E(\rho_0, P_0)$ in Eqns (1)–(3) corresponds to the principal shock Hugoniot.

To control the thermal constituents of the material's EOS, Ya B Zel'dovich came up with the idea [11, 12] of conducting shock wave experiments on samples with an artificially lowered initial density $\rho_{00} = \rho_0/m$ (where the porosity factor $m > 1$). In practice, such samples are made of a powder-like material, which consists of small particles separated by hollow spaces. The initially heterogeneous substance is assumed to become homogeneous behind the shock front. In going from the experimental dependence $D(U)$, which corresponds to a substance with a fixed value of m, to its shock Hugoniot in the (P, σ) variables, the relatively small surface energy of dispersing the initial sample is neglected in Eqns (1)–(3) (i.e. it is assumed that $E_{00} = E_0 = \text{const}$), as is the quantity P_{00}. The shock $P(\sigma)$ dependences so derived, which correspond to different m, are employed in the selection of parameters of model EOSs for the substance under study in the domain of states realized in experiments.

In experimentation with porous samples, D and U are usually determined under conditions when the shock wave, which is produced by a special loading device (a shock wave generator), initially travels over a screen and subsequently gives way to an immediately adjacent porous sample. As this takes place, either a centered rarefaction wave or a reflected shock wave (depending on the ratio between the dynamic stiffnesses of the screen material and the porous substance under investigation) travels into the screen from the interface between the substances. The shock wave velocity D in the sample is determined by measuring the wave transit time between sensors (electrical contacts, piezoelectric sensors, etc.) positioned at certain intervals. The value of U is mostly determined by the reflection technique [13], in which the second experimentally examined quantity, apart from velocity D in the sample, is the wave velocity D in a reference screen with the EOS well known from independent experiments. These reference substances are usually Al, Fe, and Cu. All desired parameters of the wave traveling over the screen are determined from the resultant value of D in the screen and the known EOS of its substance. After that, with recourse to the $P-U$ diagram technique, it is possible to find the value of U in the porous substance under investigation (from the known initial density ρ_{00} and the resultant shock wave velocity D in the sample).

In the investigation of porous samples in laboratory conditions at the Russian Federal Nuclear Center — All-Russian Research Institute of Experimental Physics (RFNC–VNIIEF), advantage is taken of different shock generators, which are based on the acceleration of metal impactors-liners by the explosion products of condensed explosives to velocities of $\approx 0.3-9$ km s^{-1}. Their description is given elsewhere [6, 14]. Some initially porous substances were also studied with the employment of shock waves generated by underground nuclear explosions.

Among porous substances, the powders of metals and quartz were most amply studied, with the execution of several methodical measurements. Methodical experiments were carried out, in particular, to elucidate the effect of particle

size on the measurement data. It turned out that particle size variations for metals in the $\approx 0.01-100$-μm range [15–18] and quartz in the $\approx 10-300$-μm range [19] had no effect, to within the accuracy of measurements, on the velocity D in samples with a fixed initial porosity m at relatively high pressures ($> 5-10$ GPa). The possible influence of humidity and the air residing in the powder pores were also investigated [16, 19]. However, no significant effect of humidity and in-pore air (from experiments with 'natural' and carefully dried samples; evacuation from a pressure of 1 atm to ≈ 1 mmHg) on the D value was revealed. In methodical experiments on porous copper, an investigation was made of the effect of sample thickness [20], which was varied by more than an order of magnitude (from several millimeters to several centimeters). These experiments yielded practically the same results. Also, the shock wave profile in porous quartz was recorded with a manganin sensor [19]. The recorded stationary profile was in qualitative agreement with the results of similar measurements in initially continuous homogeneous materials. The data given above evidence the possibility of using the data of shock wave experiments with porous samples, including those carried out in the framework of a simplified formulation (in particular, without drying and evacuation), to determine the EOS of a substance under investigation.

In the laboratory experiments performed on porous substances at the RFNC–VNIIEF, every experimental point, as a rule, results from averaging the data obtained in a series of 4–6 independent experiments. The accuracy of its parameters is estimated as follows: $|\Delta D/D| \approx 1\,\%-2\,\%$, $|\Delta U/U| \approx 1\,\%-2\,\%$, and $|\Delta\sigma/\sigma| = m\sigma(\sigma-1)\times(|\Delta D/D| + |\Delta U/U|)$.

3. Results of experiments with metals

Zel'dovich [11] predicted the run of the shock Hugoniots of an initially porous substance proceeding from the Mie–Grüneisen EOS (see also monograph [12]):

$$P = P_{\text{cold}}(V) + \frac{\gamma}{V}\left(E - E_{\text{cold}}(V)\right). \tag{4}$$

Here, P_{cold} is the 'cold' pressure (at an absolute temperature $T = 0$), and $E_{\text{cold}}(V) = -\int_{V_0}^{V} P_{\text{cold}}(V)\,\mathrm{d}V$, where $V_0 = 1/\rho_0$. The Grüneisen coefficient appearing in formula (4), defined by the relation

$$\gamma = V\left(\frac{\partial P}{\partial E}\right)_V, \tag{5}$$

was assumed to be positive and constant. Equation (4) is based on the assumption of small harmonic particle oscillations, which is valid for relatively low temperatures. With neglect of the small difference between the substance properties at $T = 0$ and $T = 298$ K, the substitution of Eqn (4) into Eqns (1)–(3) leads to the following expression for the impact pressure:

$$P = \frac{(h-1)\,P_{\text{cold}} - 2\rho_0\sigma E_{\text{cold}}}{h - m\sigma}, \tag{6}$$

where $h = 1 + 2/\gamma$. For many metals at close-to-normal conditions, the coefficient $\gamma \approx 2$, to which $h \approx 2$ corresponds. The shock Hugoniots calculated on the basis of expression (6) in the (P, σ) coordinates, which correspond to four different porosities ($m = 1, m_1 < h, m_2 = h, m_3 > h$), are qualitatively depicted by solid curves in Fig. 2 (the calculated curves are characterized by $P = 0$ in the initial portions, in the σ intervals from $1/m$ to 1). Each of the Hugoniots in Fig. 2 corresponds to its own value of the limiting compression h/m, whereby the denominator in expression (6) becomes zero. For $m < h$ (the m_1 mode), the Hugoniots are located in the domain $\sigma > 1$, and for $m > h$ (the m_3 mode) in the domain $\sigma < 1$. The latter is attributable to such strong substance heating and its consequential strong thermal expansion at high m values that the substance cannot compress to normal density ρ_0 under the pressure applied.

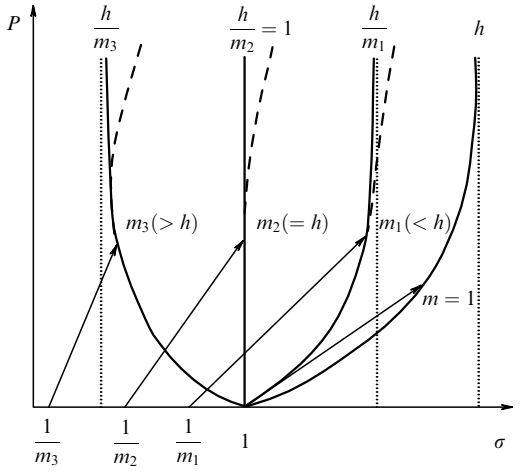

Figure 2. Schematic representation of the shock Hugoniots of an initially continuous substance and initially porous ones for different porosity factors m. The solid lines depict the dependences calculated on the basis of the Mie–Grüneisen EOS, and the dashed lines are the experimental departures from the calculated dependences.

The first experiments were executed with porous Fe having $m \approx 1.41$ [21]. The shock compression mode m_1 (see Fig. 2) was realized for $P \approx 100-300$ GPa, and $\sigma \approx 1.2-1.4$. The experiments permitted estimating γ for Fe in this state domain and refining its EOS.

Porous W with $m \approx 1.7-4.3$ was investigated in the range $P \approx 20-400$ GPa in Ref. [22]. By and large, the experimental Hugoniots corresponded to the model dependences plotted in Fig. 2. Experimental realization of the mode m_3 (for $m > 2.1$) confirmed a rather unusual inference of the theory that shock compression may give rise to states characterized by $\sigma < 1$. At the same time, the positions of experimental Hugoniots at high pressures exhibited small deviations towards higher σ from the model dependences defined by expression (6). These departures, which are qualitatively illustrated by dashed curves in Fig. 2, were attributed to a lowering of γ with an increase in T. The existence of such deviations was indicative of the necessity of correcting the EOS (4) in the domain of high substance heating. The temperature estimates (up to $\approx 3\times10^4$ K) made in Ref. [22] suggested that the deviations occurred in the existence domain of the W liquid state.

In Ref. [15], a study was made of the shock compressibility of four porous metals: Al ($m \approx 1.43$, 2.08, 2.98), Ni ($m \approx 1.43$, 1.75, 3.00), Cu ($m \approx 1.57$, 2.00, 3.01, 4.00), and Pb ($m \approx 1.67$). The highest pressure in the last three metals was ≈ 800 GPa. As in Ref. [22], both compression modes (m_1 and m_3) were realized and an appreciable 'softening' (the dashed curves in Fig. 2) of experimental shock adiabats was revealed in the melt domain. It should be noted that the values of shock wave parameters published in Ref. [15] were later refined by A I Funtikov. The refined quantities for Ni were

given in Ref. [16], and for Cu in Ref. [20]. For Pb, the changes were small. The updated (P, σ) characteristics of porous Al are presented below in Fig. 5.

A new form of a wide-range EOS of a liquid was used to describe experimental data in Ref. [15]. This model was underlain by V P Kopyshev's idea [23, 24] about how to interpolate the thermal constituent of the free energy of an atomic system between the low-temperature (small atomic vibrations) and high-temperature (monatomic ideal gas with $\gamma = 2/3$) state domains. In this case, the cold EOS constituents are assumed to be known. With the inclusion of the contribution from thermal electron excitation, this model permitted, for the appropriate selection of free constants, describing the experimental data for all metals investigated in Ref. [15]. From the initial letters of the surnames of the three first authors of Ref. [15] — Kormer, Urlin, and Funtikov — this model has come to be known as the KUF EOS.

We emphasize that the KUF interpolative equation has played the decisive role in the formation of one of approaches to the construction of wide-range semiempirical EOSs. The ideas underlying this approach are also used, in a modified form, in more recent equations [25–27].

The number of investigated metals and the number of porous shock Hugoniots determined for each of them were substantially increased in Refs [16–18, 20, 28–36], in which data were obtained for Mg, Al, Ti, V, Cr, Fe, Ni, Cu, Zn, Mo, Sn, Ta, W, Pb, Bi, and U. The data of these, as well as of a number of other studies, are collected in reference book [10]. The most comprehensive studies were made on Ni (13 Hugoniots), Cu (9 Hugoniots), and Mo (8 Hugoniots). Measurements for maximal porosity factors ($m \geqslant 10$) were made for Fe, Ni, and Cu, which permitted realizing the mode of significant ($\sigma \approx 0.2-0.4$) high-temperature substance expansion.

Figure 3 shows the experimental $D(U)$ dependences for Ni at different m. The shock Hugoniots diverge in a fan-shaped manner from the starting point with coordinates $U = 0$, $D_0 \approx 0.1$ km s^{-1}. For $U \approx 0$, the slopes $(\mathrm{d}D/\mathrm{d}U)_m$ of the Hugoniots are appreciably different. For relatively small m, the slopes are ≈ 3, for $m \approx 3-5$ they are approximately 1.2, and for $m > 7$ they are about 1. With increasing U, the values of $(\mathrm{d}D/\mathrm{d}U)_m$ for different-m Hugoniots gradually equalize and approach the slope of the principal shock adiabat at $m = 1$. The experimental $D(U)$ dependences for other metals behave in the qualitatively same way.

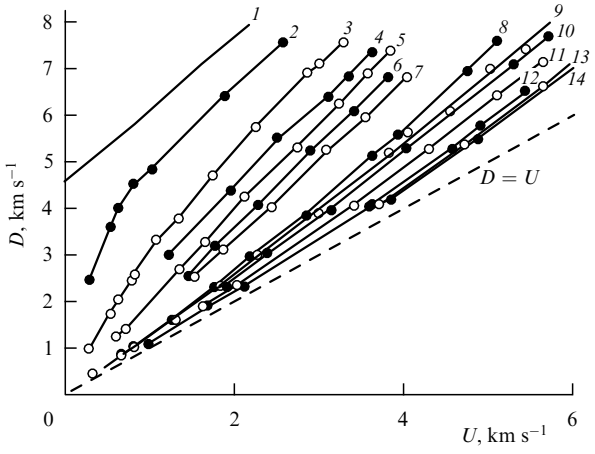

Figure 3. Experimental shock Hugoniots *1 – 14* of continuous and porous Ni for respective porosity factors m: 1.00, 1.10, 1.41, 1.72, 2.00, 2.30, 2.70, 4.55, 5.58, 7.20, 10.0, 15.0, 20.0, and 28.0 [10].

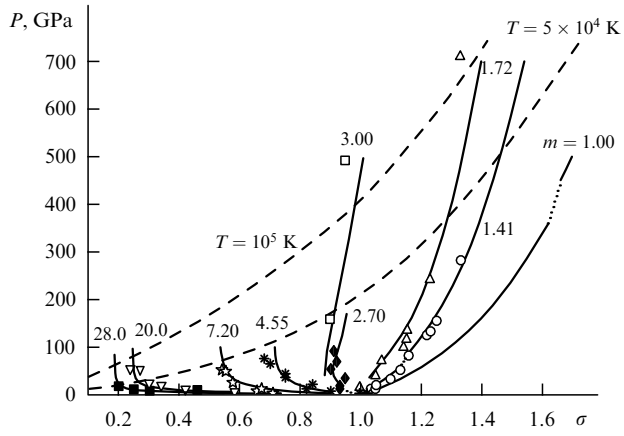

Figure 4. Shock Hugoniots of continuous and porous Ni. The experimental data from Ref. [10] for different porosity factors m are marked off by different symbols. The solid curves display the calculated shock Hugoniots for substances in solid (low P) and liquid (high P) states; the dotted portions of shock Hugoniots correspond to the phase mixture domain. The experimental values of m are indicated alongside the adiabats. The dashed curves show the calculated isotherms.

The data on the shock compression of porous Ni are given in the (P, σ) coordinates in Fig. 4. Similar results (supplemented with a number of data borrowed from Refs [8, 9]) for Al, Fe, and Cu are demonstrated in Figs 5–7. For greater clarity, several experimental shock adiabats corresponding to intermediate values of m are not shown in Figs 4–7 (for the same reason some data from Ref. [9] are omitted from Figs 6 and 7).

The shock compression of porous metals was investigated in Refs [16–18, 20, 29–36] not only in the high-pressure region, but also at relatively low 'packing' pressures. As is evident, for instance, from Figs 5–7, to compress porous metals with $m \approx 8-10$ from the initial density ρ_{00} ($\sigma = 1/m$) to a density of about $(0.7-0.8)\,\rho_0$ requires rather high (up to ≈ 5 GPa) pressures (compressive stresses). This is due to the rheology (strength) effect in the packing of powders.

A characteristic property of porous metals, which manifests itself at relatively high pressures for all the metals investigated, consists in a sequential lowering of the experimentally determined σ values (see Figs 4–7) and, accordingly, in an increase in V with increasing m in arbitrary isobars, i.e. in the positivity of the derivative $(\partial V/\partial V_{00})_P$.

In the laboratory experiments considered above, investigations were made of the domain of states with an internal energy (its increment) of up to ≈ 50 kJ g^{-1}. Higher-energy parameters (for internal energies up to ≈ 300 kJ g^{-1}) were realized in the shock compression of porous samples in underground nuclear explosions. In these experiments, investigations were carried out of Cu ($m \approx 3.10$, 4.00) [37], Fe ($m \approx 3.27$, 3.46) [20], W ($m \approx 3.08$) [20], and U ($m \approx 3.3$). The results for Cu, Fe, and W are given in Fig. 8. As in laboratory experiments, measurements in this case were made by the reflection technique with the Al screen. The data presented in Fig. 8 were obtained with the use of the $D(U)$ dependence for Al ($\rho_0 = 2.71$ g cm^{-3}) in the form $D = 6.541 + 1.158U$ [km s^{-1}] and the 'specular' approximation in the (P, U) variables for the unloading isentrope and the shock Hugoniot of Al double compression. The shock Hugoniot of Al in the (P, σ) coordinates, corresponding to

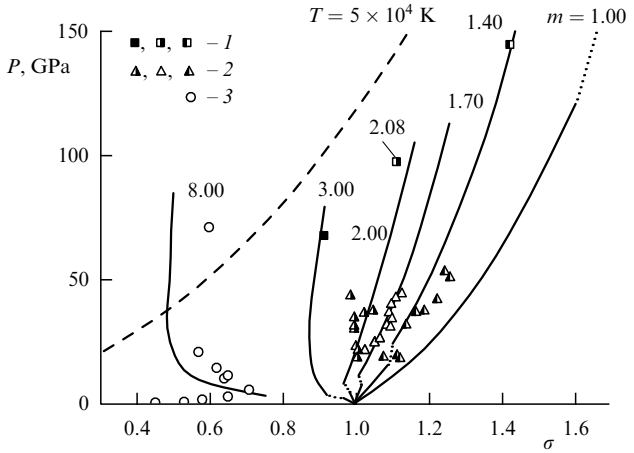

Figure 5. Same as in Fig. 4, but for Al: *1* – experimental data of Ref. [15] (processed by A I Funtikov), *2* – Ref. [8], and *3* – Ref. [10].

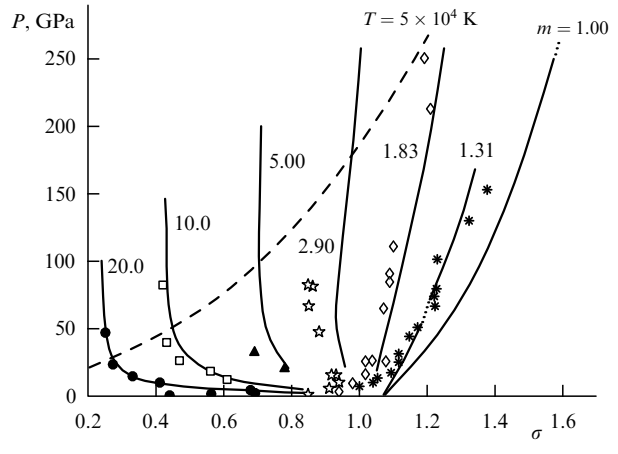

Figure 6. Same as in Fig. 4, but for Fe: experimental data of Ref. [10], with the exception of the data for $m = 1.31$ taken from Ref. [9].

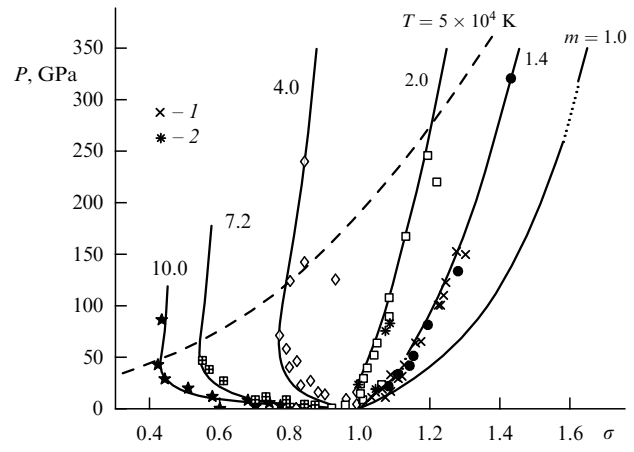

Figure 7. Same as in Fig. 4, but for Cu: experimental data of Ref. [10], with the exception of *1* ($m = 1.41$) and *2* ($m = 1.98$) data taken from Ref. [9].

this $D(U)$ dependence, is plotted in Fig. 8, which also shows experimental data on the shock compression of Al.

By and large, the data for porous metals obtained in strong shock waves produced by nuclear explosions are consistent with the data of laboratory experiments. Their combined representation in the (D, U) variables confirms the

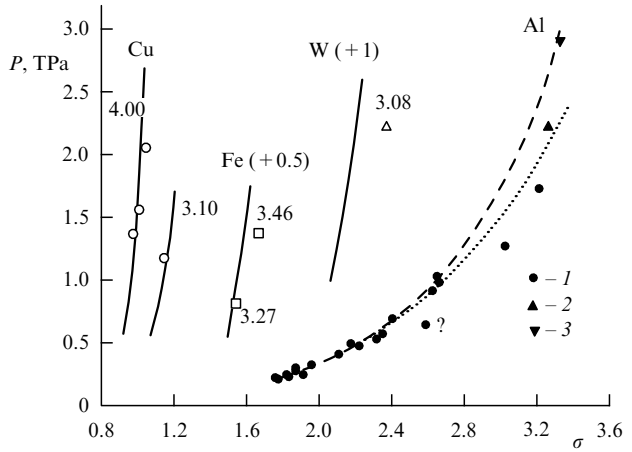

Figure 8. Shock Hugoniots of porous Cu, Fe, W and continuous Al. Experimental data for the porous metals were taken from Ref. [10]. Experimental data for continuous Al: *1* – Ref. [10], *2* – Ref. [38], and *3* – Ref. [39]. Model Hugoniots: solid curves stand for the porous metals, and the dashed curve stands for continuous Al. The dotted curve is the shock adiabat of Al calculated from the dependence $D = 6.541 + 1.158U$. The numbers alongside the adiabats indicate the porosity factor m. The data for Fe and W are shifted to the right by 0.5 and 1, respectively.

previously reached conclusion (in the discussion of Fig. 3 for Ni) that the slopes $(\mathrm{d}D/\mathrm{d}U)_m$ of the shock Hugoniots of porous metals at relatively high U are approximately equal to the slope of their principal Hugoniots. Here, the typical slopes amount to $\approx 1.2-1.3$.

The average values of $\gamma = V\Delta P/\Delta E$ (where ΔP, ΔE are the pressure and energy differences between the shock Hugoniots of porous and continuous substances for a fixed value of V) for Cu, Fe, and W, calculated from the data given in Fig. 8, are $\approx 0.6-0.7$, which is approximately three times smaller than the γ values for these metals under normal conditions.

To summarize, it is valid to say that over an approximately 60-year period of research a wealth of experimental data on the shock compression of a large number of initially porous (in some cases with $m \approx 10-30$) metals has been obtained at pressures of up to ≈ 1 TPa in a wide range of final densities, including the domain of significant substance expansion (for several metals up to $1/\sigma \approx 5$). These experimental data enabled determining the general laws of behavior of these substances under shock compression. The results of these investigations yielded substantial information about the thermal constituents of metal EOSs and lent impetus to the construction of new wide-range EOS models. One of these models is outlined in Section 4.

It should be noted that the shock compression of porous samples permitted investigating, apart from substance properties at relatively high densities, their characteristics in a relatively low-density state (close to the domain of evaporation) by the isentropic unloading technique. This possibility arises from a greater increase in substance entropy behind the shock front in a porous substance compared to that along the principal shock adiabat. Several initially porous metals have been studied by this technique. By way of example, Fig. 9 demonstrates the experimental data on the isentropic unloading of Cu. The nonmonotonic behavior of the dependences is due to substance evaporation in the unloading wave.

Along with metals, other porous substances have also been extensively studied at the RFNC–VNIIEF, in particular

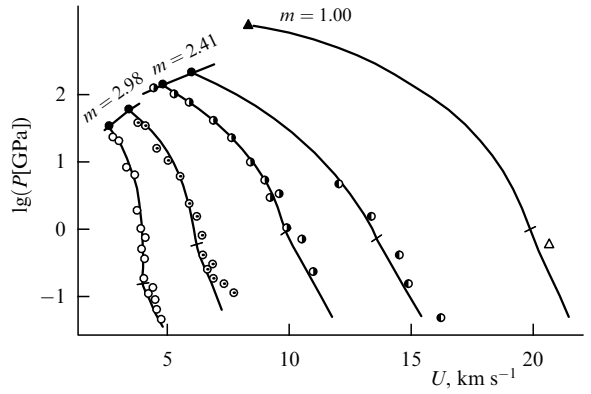

Figure 9. Unloading isentropes of initially porous and continuous copper for different porosity factors m. Experimental data for $m = 1$ were borrowed from Ref. [40], for $m = 2.41$ and 2.98 from Ref. [26]. The curves result from calculations based on a model EOS. Slanting segments indicate the onset of evaporation in the unloading wave.

ion salts, carbon, and water in a solid state (snow). Generally, the substances listed exhibit the same properties of shock compression as porous metals $\left((\partial V/\partial V_{00})_P > 0\right)$. The data obtained for these and some other porous substances are contained in reference book [10].

4. Model description of the experimental data for metals

To describe experimental data, including those on the shock compression of porous samples, use is made of different semiempirical model EOSs of metals. These EOSs are reviewed in several papers [23, 41–43]. The series of KUF type EOSs was mentioned in Section 3. Model EOSs contain free constants determined by best fitting to experimental data. Preference is given to those EOSs which reproduce a greater amount of data for a smaller number of the constants and also exhibit correct asymptotic behavior under extreme (P, T) conditions.

Below, we describe a semiempirical model EOS [44–48] which takes into account evaporation, thermal ionization, and melting of a substance and contains a relatively small set of free parameters determined from available experimental data. In this case, there is satisfactory agreement with the results of other dynamic experiments, in particular, on the shock compression of porous metal samples (these experiments are not employed in the determination of the model's constants).

In the formulation of the model of a liquid, the latter is treated as a gas of particles (atoms, ions, electrons); the real liquid properties (evaporation, finite compressibility, etc.) are described by introducing corrective additional terms (reflecting the existence of particle 'size', interparticle attraction, etc.) into the thermodynamic functions of an ideal gas. In this respect, the model is close to the chemical plasma model [49], which proved to be applicable for describing the properties of shock-compressed porous metals [18, 50]. In comparison with the model of Ref. [49], however, the model under consideration is mathematically simpler and contains a smaller number of free constants, which is of importance for practical applications.

To describe liquids and gases with the inclusion of ionization processes, use is made of a modified Van der Waals (mVdW) model. The thermal equation of state may be represented (with the introduction of an additional variable $P^{\rm rep}$) in the following parametric form:

$$P = P^{\rm rep} + P^{\rm att}\left(\bar{V}, \{N\}\right), \tag{7}$$

$$P^{\rm rep} = \frac{N k_{\rm B} T}{\bar{V} - \bar{V}_{\rm C}}, \tag{8}$$

$$\bar{V}_{\rm C} = \bar{V}_{\rm C}\left(P^{\rm rep}, \{N\}\right). \tag{9}$$

Here, $k_{\rm B}$ is the Boltzmann constant; $N = \sum_i N_i + N_{\rm e}$ is the total number of particles equal to the sum of the numbers of ions N_i (i is the ion sort) and electrons $N_{\rm e}$ contained in a volume $\bar{V}$, and the set of N_i, $N_{\rm e}$, which defines the mixture composition, is defined as $\{N\}$; $P^{\rm att}$ is the attraction pressure; $\bar{V}_{\rm C}$ is the covolume, and $P^{\rm rep}$ is the kinetic pressure. It is assumed that $P^{\rm rep}$ is the cause of particle compression, which is reflected in formula (9) (in which the possible dependence of the covolume on $\{N\}$ is also included). The functions $P^{\rm att}$ and $\bar{V}_{\rm C}$ are empirical. The variables of the EOS in the mVdW model are T, $P^{\rm rep}$, and $\{N\}$. When these variables are set, $\bar{V}$ is found from expression (8), after which P is obtained from expression (7). In this way, a thermal $P-T-\bar{V}$ relation is determined. For $\bar{V}_{\rm C} = {\rm const}$ and $N_{\rm e} = 0$, the modified VdW model turns into the initial VdW model and, like the latter, includes evaporation.

The free energy $\bar{F}$ of a mixture is determined simultaneously with formulas (8), (9) utilizing the following expression

$$\bar{F} = \bar{E}^{\rm rep}\left(P^{\rm rep}, \{N\}\right) + \bar{E}^{\rm att}\left(V, \{N\}\right) - k_{\rm B} T \sum_i N_i \ln\left(\frac{{\rm e} N T^{5/2} r_i \sigma_i(T)}{N_i P^{\rm rep}}\right) - k_{\rm B} T N_{\rm e} \ln\left(\frac{2{\rm e} N T^{5/2} r_{\rm e}}{N_{\rm e} P^{\rm rep}}\right), \tag{10}$$

where e is the base of a natural logarithm, and

$$\bar{E}^{\rm rep} = -\int_0^{P^{\rm rep}} P^{\rm rep}\left(\frac{\partial \bar{V}_{\rm C}\left(P^{\rm rep}, \{N\}\right)}{\partial P^{\rm rep}}\right)_{\{N\}={\rm const}} {\rm d}P^{\rm rep}, \tag{11}$$

$$\bar{E}^{\rm att} = -\int_{\infty}^{\bar{V}} P^{\rm att}\left(\bar{V}, \{N\}\right)_{\{N\}={\rm const}} {\rm d}\bar{V}, \tag{12}$$

$r = k_{\rm B}^{5/2}(m/2\pi\hbar^2)^{3/2}$, m is the particle mass, $\hbar$ is the Planck constant, and $\sigma(T)$ is the internal statistical sum of an individual particle. Integrals (11) and (12) are taken for $\{N\} = {\rm const}$.

From variables T, $P^{\rm rep}$, and $\{N\}$, it is possible to calculate, along with $\bar{F}$, the entropy $\bar{S} = -(\partial\bar{F}/\partial T)_{\bar{V},\{N\}}$, the energy $\bar{E} = \bar{F} + T\bar{S}$, the pressure $P = -(\partial\bar{F}/\partial\bar{V})_{T,\{N\}}$ [coincides with expression (7)], etc.

The dependences of $\bar{V}_{\rm C}$ and $P^{\rm att}$ on the degree of ionization were disregarded in the concrete application of the model to metals. It was assumed that

$$\bar{V}_{\rm C}\left(P^{\rm rep}, \{N\}\right) = M V_{\rm C}(P^{\rm rep}), \tag{13}$$

$$P^{\rm att}\left(\bar{V}, \{N\}\right) = P^{\rm att}\left(\frac{\bar{V}}{M}\right) = P^{\rm att}(V), \tag{14}$$

where $M = m_0 \sum_i N_i$ is the substance's mass, m_0 is the atomic mass (the electron mass is neglected owing to its smallness in

comparison with ion masses, as is the difference between the masses of various ions), V is, as above, the specific volume (of unit mass), and V_C is the specific covolume.

If, instead of dependence $V_C(P^{rep})$ in expression (13), use is made of its inverse function $P^{rep}(V_C)$, relations (7)–(9) can be written out in variables T, V_C as

$$P = P^{rep}(V_C) + P^{att}(V)\,, \tag{15}$$

$$\bar{V} = \bar{V}_C + \frac{Nk_BT}{P^{rep}(V_C)}\,. \tag{16}$$

At $T = 0$, it follows from relation (16) that $\bar{V} = \bar{V}_C$, $V = V_C$, and in this case relation (15) represents the equation for cold pressure P_{cold}:

$$P_{cold}(V) = P^{rep}(V) + P^{att}(V)\,. \tag{17}$$

In the realistic selection of the dependences $P^{att}(V)$ and $P^{rep}(V_C)$ [or, which is equivalent, $V_C(P^{rep})$ instead of $P^{rep}(V_C)$], it is possible with the aid of Eqn (17) to describe the characteristic properties of liquid compression at relatively low T (in particular, the shock compressibility of a liquid), which extends the VdW model to the high-density region.

In the state of thermodynamic equilibrium, the values of N_i and N_e are found from the equations $\mu_i = \mu_{i+1} + \mu_e$ for the particle chemical potentials $\mu_k = (\partial\bar{F}/\partial N_k)_{\bar{V},T,\{N\}_{(\neq k)}}$ ($k = i$, e; the derivative is calculated for a constant number of particles of all components except the kth one). The final equations are similar to the Saha equations (differing from them by the change $P \to P^{rep}$) and turn into them for V, $T \to \infty$ (in this limit $P^{att} = 0$, $P = P^{rep}$). In the latter case, the model described by Eqns (7)–(10) reduces to the EOS of the mixture of ideal ion and electron gases.

In the concrete construction of the EOSs of metals, statistical sums σ were limited to the inclusion of the ground particle's states. The statistical weights and ion ionization potentials belong to reference data.

Therefore, in view of the assumptions made above, the liquid and gas model is completely defined by specifying empirical functions $V_C(P^{rep})$ [or $P^{rep}(V_C)$] and $P^{att}(V)$.

Possible polymorphous phase transitions are disregarded in the consideration of the solid state. For F in the solid phase, use is made of an expression which follows from the theory of small atomic vibrations for the temperature interval $T \geqslant \Theta_D$ (where Θ_D is the effective Debye temperature):

$$F = E_{cold}(V) + 3N_0k_BT\ln\left(\frac{\Theta_D(V)}{T}\right), \tag{18}$$

where $N_0 = \text{const}$ is the number of atoms in a volume V, and E_{cold} is the cold energy.

The liquid and solid phase models are united as follows. The liquid EOSs (7)–(10), (13), (14), the dependence $\Theta_D(V)$, and the melting temperature $T^m(P)$ are assumed to be known. From them and from the liquid (S^l) and solid (S^s) phase entropies in the melting curve [the superscripts l (liquid) and s (solid) pertain to the quantities in this curve], using the Clausius–Clapeyron equation

$$\frac{dT^m}{dP} = \frac{S^l - S^s}{V^l - V^s}\,, \tag{19}$$

it is possible to find the dependence $V^s(P)$. After this, the function E_{cold} entering expression (18) is determined from the condition that the Gibbs potentials $\Phi(P,T) = F + PV$ of the phases are equal in the melting curve. The solid-phase EOS is thereby completely defined in a consistent way.

For a melting criterion, use is made of an analog of the Lindemann criterion. The volume of a liquid in melting is assumed to satisfy the condition

$$\frac{V^l - V_C(P^{rep})}{V_C(P^{rep})} = \beta = \text{const}\,. \tag{20}$$

Equations (7)–(9), (13), (14), and (20) permit calculating the dependence $T^m(P)$.

The simplest variables of a complete model EOS are T, P^{rep} (or V_C). When $T > T^m$, calculations are performed using the liquid EOS, otherwise utilizing the solid-state EOS. In two-phase domains, use is made of a conventional additive approach.

The dependences $P^{att}(V)$, $V_C(P^{rep})$, and $\Theta_D(V)$, which define the complete EOS, are represented by rather simple functions containing a relatively small number of free constants which [along with β in expression (20)] are selected proceeding from the model description of thermodynamic substance's characteristics at atmospheric pressure (the densities and compressibilities at room temperature, the melting temperatures and enthalpies, the binding energies) and the principal shock Hugoniot. The detailed form of the EOS and the parameters for Al, Fe, Ni, Cu, Mo, Ta, W, and Pb are given in Refs [45, 46].

Figures 4–8 show the results of describing experiments with porous Ni, Al, Fe, Cu, and W samples. On the whole, the model dependences agree well (with an error in compression ratio close to the uncertainty of measurements) with the data of experiments without special normalization to them throughout the domain of the (P, σ) states investigated. The calculated temperature values amount to $\sim 10^5$ K. The highest ($\approx 3 \times 10^5$ K) is realized for Cu with $m = 4$ at $P \approx 2$ TPa. In this case, the calculated degree of ionization equals ≈ 2.7. For other porous metals investigated, the model experiment description is close to that presented in Figs 4–8.

The EOS also provides a satisfactory description of the data of other experiments on metals, including those on the isentropic unloading of initially continuous and porous samples (this is illustrated in Fig. 9 for Cu), melting under shock compression and isentropic unloading, the speed of sound behind the shock front, and static isothermal ($T = 300$ K) compression (the results of comparisons are outlined in Refs [44–47]; Refs [45, 46] report on the parameters of the critical points for eight metals).

5. Relation between the Grüneisen coefficient and the relative position of porous shock Hugoniots

In this section we give the relations which permit judging the sign of Grüneisen parameter γ (5) of a substance, which is an important characteristic of its EOS, by the relative arrangement of the shock Hugoniots of porous samples in (P, V) coordinates (relative to each other and to the principal Hugoniot). In the derivation of these relations, we assume that equilibrium thermodynamics applies to the description of dynamic experiments. The data of experiments with metals testify to the positivity of γ for metals. On the contrary experiments on silicates exhibit a different tendency (see Section 6).

The availability of data on the shock compression of continuous and porous samples of a substance permits calculating on their base the following parameter (or estimating its average value by a difference technique)

$$\lambda = \left(\frac{\partial V}{\partial V_{00}}\right)_P , \tag{21}$$

where $V = V(P, V_{00})$ is the specific volume of the substance in the state corresponding to the shock Hugoniot with given P and $m = V_{00}/V_0$. As noted in Section 3, metals are characterized by $\lambda > 0$.

Let us show that the sign of λ is determined by the sign of γ. To do this, we take advantage of the coefficient

$$\eta = P\left(\frac{\partial V}{\partial E}\right)_P , \tag{22}$$

which, in view of the thermodynamic relations $\mathrm{d}E = T\,\mathrm{d}S - P\,\mathrm{d}V$, $(\partial S/\partial V)_P = (\partial P/\partial T)_S = c_s^2/\gamma V T$ (where $c_s = V\sqrt{-(\partial P/\partial V)_S}$ is the speed of sound), may be written out as

$$\eta = \frac{P}{\rho c_s^2/\gamma - P} , \tag{23}$$

whence we obtain

$$\gamma = \frac{\eta \rho c_s^2}{P(1+\eta)} . \tag{24}$$

Differentiating relation (3) and making some transformations, which are omitted here, we arrive at the following expression for η in terms of λ:

$$\eta = \frac{2\lambda}{2(\mathrm{d}E_{00}/\mathrm{d}V_{00})/P + 1 - \lambda} . \tag{25}$$

Substitution of expression (25) into formula (24) gives

$$\gamma = \frac{2\lambda \rho c_s^2}{P\bigl(1 + \lambda + 2(\mathrm{d}E_{00}/\mathrm{d}V_{00})/P\bigr)} . \tag{26}$$

For relatively large P, the quantity $2(\mathrm{d}E_{00}/\mathrm{d}V_{00})/P$ may ordinarily be neglected (for porous samples, $\mathrm{d}E_{00}/\mathrm{d}V_{00} = 0$) and formula (26) takes on the form

$$\gamma = \frac{2\lambda \rho c_s^2}{P(1+\lambda)} . \tag{27}$$

In the mutual arrangement of the shock adiabats characterized by different m values, three versions are possible, which correspond to $\lambda > 0$, $\lambda = 0$, and $\lambda < 0$. According to formula (27), γ values of different signs correspond to them. For $\lambda > 0$, the condition $\gamma > 0$ is fulfilled (metals and several other substances). If $\lambda = 0$, then $\gamma = 0$. In this case, a substance with different m values is compressed to the same volume V under a similar pressure of magnitude P. For $\lambda < 0$ ($|\lambda| < 1$), parameter $\gamma < 0$. The manifestation of this property by the substance can, in particular, qualitatively explain the unusual situation wherein the value of V realized in the shock compression of a substance with $m > 1$ is smaller than the value of V obtained in the Hugoniot with $m = 1$ (i.e. shock Hugoniots with different m intersect).

The $\lambda > 0$ ($\gamma > 0$) property, which manifests itself in experiments on porous metals, is consistent with the data on the shock compression of initially liquid metals possessing a lower initial density in comparison with ρ_0 [51]. The shock Hugoniots of Zn, Sn, Cd, and Pb melts in the (P, V) coordinates are located to the right of the principal shock Hugoniots of these metals (these adiabats coincide to within experimental error for Cu). The same property ($\lambda > 0$) also shows up, for instance, in the shock compression of Mo initially heated to a temperature of 1673 K [52]. According to the estimates of Refs [51, 52], the average values of $\gamma \sim 1$ are typical for the metals listed above.

Experiments on double shock-wave loading from the initial states corresponding to the principal shock Hugoniot also yield positive γ values for metals (Al, Mg, Zn [10]). In the (P, V) coordinates, these data lie to the left of the principal Hugoniot (curve HH in Fig. 1 sloping gently relative to the Hugoniot $H_{m=1}$). This position of the indicated dependences is attributable to the higher values of E and T (for $V = \mathrm{const}$) realized under single shock compression compared to these quantities in the double compression, which leads to a greater pressure increment in the former case for $\gamma = V(\partial P/\partial E)_V > 0$. In the case of metals, the same factor accounts for the location of unloading isentropes to the right of single-compression shock adiabats (for instance, the gently sloping isentrope S_1 in comparison with the Hugoniot $H_{m=1}$ in Fig. 1).

It should be noted that in single-phase states the coefficient γ is related to the thermal expansion coefficient $\beta = (\partial V/\partial T)_P/V$, the isobaric heat capacity $C_P = T(\partial S/\partial T)_P > 0$, and the speed of sound c_s by the expression

$$\gamma = \frac{\beta c_s^2}{C_P} . \tag{28}$$

In the domain of the mixture of two (1 and 2) phases possessing an equilibrium curve $T^{12}(P)$, the following relationship holds true:

$$\gamma = \frac{\rho c_s^2\, \mathrm{d}T^{12}(P)/\mathrm{d}P}{T^{12}(P)} . \tag{29}$$

One can see from relations (28), (29) that the realization of the $\gamma > 0$ characteristic in single-phase state domains, which occupy the main part of space in the phase diagram, is associated with the manifestation of the property $\beta > 0$ by the substance, and with the slope of equilibrium curve $\mathrm{d}T^{12}(P)/\mathrm{d}P > 0$ in relatively local two-phase domains. The change in sign of the last two quantities has the consequence that $\gamma < 0$. In this case, the substance under external action exhibits properties qualitatively different from those of the metals considered above.

6. Peculiarities of dynamic experiments on silicates

In a rather broad (P, V)-state domain, different silicates exhibit tendencies contrary to those observed in experiments with metals (see Section 5).

Figure 10 demonstrates the data on the shock compression (with initial parameters $P_0 = 1$ atm, $T_0 = 298$ K) of initially continuous (coesite with $\rho_0 = 2.92$ g cm^{-3}, α-quartz and quartzite with $\rho_0 = 2.65$ g cm^{-3}, and fused silica with $\rho_0 = 2.204$ g cm^{-3}) and porous ($\rho_{00} = 1.76$, 1.90 g cm^{-3})

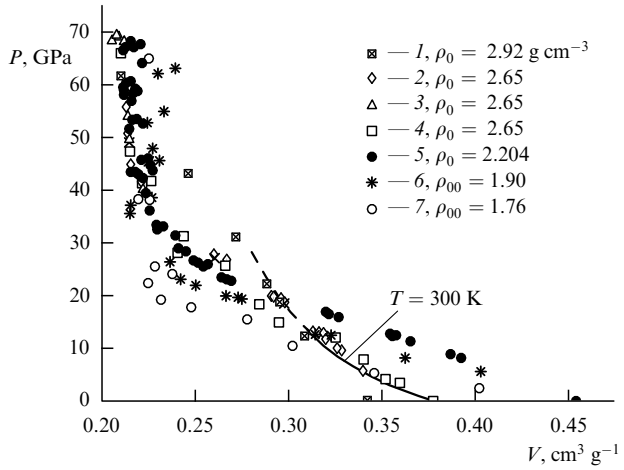

Figure 10. SiO_2 shock Hugoniots. Experimental data on shock compression: *1*, *4*, *7* – Ref. [10]; *2* – Ref. [53]; *3*, *5*, *6* – Ref. [9]. The solid curve stands for the $T = 300$ K isotherm of α-SiO_2 quartz [54] (the dashed section of the curve is an extrapolation).

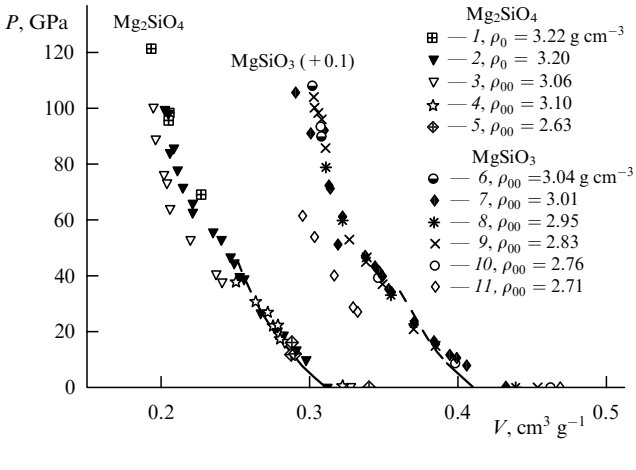

Figure 12. Mg_2SiO_4 and $MgSiO_3$ shock Hugoniots. Experimental data on shock compression: *1* – Ref. [62]; *2*, *3*, *7–11* – Ref. [9]; *4*, *5* – Ref. [63]; *6* – Ref. [64]. The solid curves are the $T = 300$ K isotherms of Mg_2SiO_4 and $MgSiO_3$ [54] (the dashed curves are extrapolations). The data for $MgSiO_3$ are shifted to the right along the abscissa by 0.1 cm³ g⁻¹.

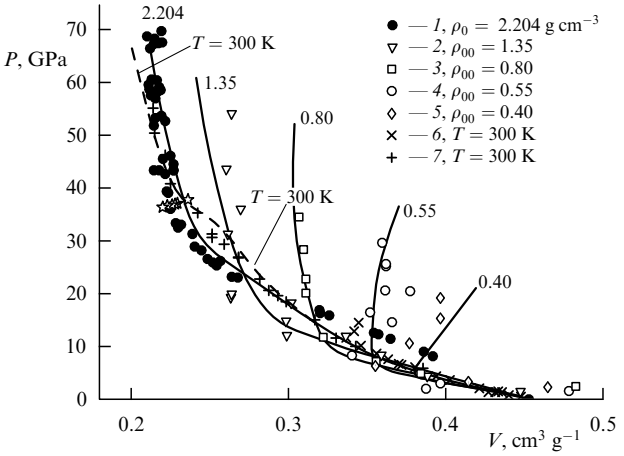

Figure 11. SiO_2 shock Hugoniots. Experimental data on shock compression: *1* – Ref. [9], *2–5* — Ref. [10]. Experimental data on the isothermal compression of fused silica with $\rho_0 = 2.204$ g cm^{-3}: *6* – Ref. [55], *7* – Ref. [56]. Results of calculations based on a model EOS: solid curves — shock Hugoniots; dashed curve — $T = 30$ K isotherm of fused silica.

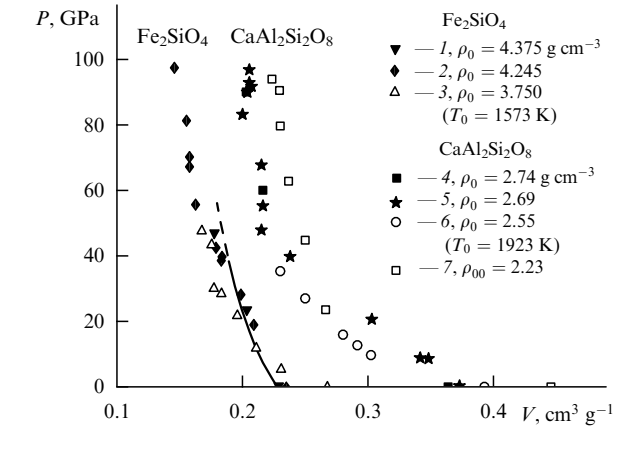

Figure 13. Fe_2SiO_4 and $CaAl_2Si_2O_8$ shock Hugoniots. Experimental data on shock compression: *1* — Ref. [65], *2* — Ref. [9], *3* – Ref. [65] (initially liquid state), *4*, *7* — Ref. [66], *5* — Ref. [67], *6* — Ref. [68] (initially liquid state). The solid curve is the $T = 300$ K isotherms of Fe_2SiO_4 [54] (the dashed curve is an extrapolation).

samples of silica SiO_2 (hereinafter the initial density of nonporous, including liquid, samples is denoted as ρ_0, and of porous ones as ρ_{00}). Figure 10 is partly complemented by Fig. 11, which gives, along with the shock compression data for fused silica, the data of experiments in the shock compression of porous SiO_2 for $\rho_{00} = 1.35$, 0.80, 0.55, and 0.40 g cm^{-3} (at the initial parameters $P_0 = 1$ atm, $T_0 = 298$ K). For clarity, the data of some experiments in the shock compression of porous samples with intermediate ρ_{00} values were omitted in Figs 10, 11.

We note that the SiO_2 shock compression data shown in Figs 10 and 11 (including those omitted) are not exhaustive. In particular, investigations in Refs [57–60] were carried out for $\rho_{00} < 0.4$ g cm^{-3} in a pressure range of up to 100 GPa, and in Ref. [61] the shock compressibility of samples with $\rho_{00} = 1.35$, 1.75 g cm^{-3} was investigated for pressures of up to ≈ 2 TPa.

Figures 12 and 13 present the results of experiments in the shock compression (initially continuous and porous solid samples with the initial parameters $P_0 = 1$ atm, $T_0 = 298$ K; melts for $P_0 = 1$ atm and an elevated temperature T_0) of forsterite Mg_2SiO_4, enstatite $MgSiO_3$, fayalite Fe_2SiO_4, and anorthite $CaAl_2Si_2O_8$.

Along with shock wave data, Figs 10, 12, and 13 depict the static compression isotherms ($T = 300$ K) of the initial phases of several crystalline silicates for moderate pressures, which were calculated using the relation $P = K_T/K'[(\rho/\rho_0)^{K'} - 1]$ with parameters borrowed from Ref. [54]: $\rho_0 = 2.65$, $K_T = 38$, $K' = 5.4$ — α-SiO_2; $\rho_0 = 3.22$, $K_T = 135.7$, $K' = 3.98$ — Mg_2SiO_4; $\rho_0 = 3.22$, $K_T = 125$, $K' = 5$ — $MgSiO_3$, and $\rho_0 = 4.39$, $K_T = 124$, $K' = 4$ — Fe_2SiO_4 (dimensionality: ρ_0 — [g cm^{-3}], K_T — [GPa]). Experimental data on the isothermal ($T = 300$ K) compression of fused silica with $\rho_0 = 2.204$ g cm^{-3} are given in Fig. 11.

It should be noted that the shock Hugoniots of continuous and slightly porous samples are located in the solid-state domain (prior to melting) in the pressure range considered in Figs 10–13. According to the estimates of Ref. [65], initially

liquid Fe_2SiO_4 (see Fig. 13) becomes solid in the states on the shock adiabat beginning with pressures of several GPa. It is likely that initially liquid anorthite (see Fig. 13) also becomes solid at similar, relatively low, pressures (the transition of initial melts to the solid state is due to a stronger temperature rise with an increase in pressure along the melting curve in comparison with the temperature growth along the shock adiabat). Highly porous SiO_2 (see Fig. 11) at relatively high shock pressures resides in the liquid state. Estimates based on the SiO_2 EOS discussed below suggest, in particular, that the temperature of samples with $\rho_{00} = 1.35$ g cm^{-3} subjected to shock compression by the pressure $P \approx 22$ GPa rises to $T \approx 3500$ K, while samples with $\rho_{00} = 0.55$ g cm^{-3} under a pressure $P \approx 5$ GPa are heated to a temperature $T \approx 3000$ K. These values of P and T approximately correspond to parameters in the SiO_2 melting curve. That is, the peculiarities of silicate behavior discussed below take place, as a rule, in the substance solid state (highly porous SiO_2 is an exception).

With reference to Fig. 10, in a rather wide pressure range the SiO_2 shock Hugoniots corresponding to lower values of ρ_0 (or ρ_{00}) are located to the left of the Hugoniots that correspond to higher values of ρ_0 (ρ_{00}), with the result that $\lambda < 0$. In particular, this mutual arrangement of the Hugoniot of fused SiO_2 with $\rho_0 = 2.204$ g cm^{-3} and the Hugoniot of α-SiO_2 and quartzite with $\rho_0 = 2.65$ g cm^{-3} takes place in the $P \approx 20-40$-GPa range, and of the Hugoniots corresponding to $\rho_{00} = 1.76$ g cm^{-3} and $\rho_0 = 2.65$ g cm^{-3} in the $P \approx 5-40$-GPa range.

For relatively low shock intensities, estimates of λ may be affected by substance strength. The relative position of the α-SiO_2 compression isotherm at $T = 300$ K and the Hugoniot with $\rho_0 = 2.65$ g cm^{-3} (see Fig. 10) shows that the strength effect along the latter is insignificant for $P > 10$ GPa. For fused SiO_2, judging by the position of its $T = 300$ K isotherm and the shock Hugoniot (see Fig. 11), the same conclusion holds for $P > 20$ GPa. It is therefore likely that the anomalous mutual arrangement of the Hugoniots of fused and initially crystalline quartz in the $P \approx 20-40$ GPa range takes place in a close-to-hydrodynamic substance state (i.e. the rheology effect is weak in the range of the $\lambda < 0$ property manifestation). Nor is strength the chief factor in the anomaly of the Hugoniots with $\rho_{00} = 1.76$ g cm^{-3} and $\rho_0 = 2.65$ g cm^{-3} for $P \approx 5-40$ GPa (because at pressures higher than $P \approx 5$ GPa the Hugoniot of porous quartz is located to the left not only of the Hugoniot of continuous quartz, but also of its $T = 300$ K isotherm which determines to a first approximation the hydrodynamic shock adiabat of continuous material at moderate heating; the inclusion of a possible strength effect along the $\rho_{00} = 1.76$ g cm^{-3} Hugoniot will only aggravate the anomalous relationship between the shock Hugoniots under consideration).

Also unconventional (see Fig. 11) is the position of the shock Hugoniots of SiO_2 with $\rho_{00} = 0.40-1.35$ g cm^{-3} relative to the $T = 300$ K isotherm of fused silica ($\rho_0 = 2.204$ g cm^{-3}): the Hugoniots lie on the left of the isotherm in a rather wide pressure range ($P \approx 5-20$ GPa). With an increase in shock wave intensities, the behavior of these porous shock Hugoniots becomes normal — they reside to the right of the $T = 300$ K isotherm.

The tendency for $\lambda \leqslant 0$ in a rather wide pressure range also manifests itself in the shock compression of porous and continuous samples of Mg_2SiO_4 (see the $\rho_{00} = 2.63-3.10$ g cm^{-3} data positions relative to the $\rho_0 \approx 3.2$ g cm^{-3} data in Fig. 12), $MgSiO_3$ (see the $\rho_{00} = 2.71-3.04$ g cm^{-3} data in the same figure), and anorthite (see the position of the experimental point with $\rho_{00} = 2.23$ g cm^{-3} at $P \approx 23$ GPa relative to the shock Hugoniot with $\rho_0 \approx 2.7$ g cm^{-3} in Fig. 13). The results of experiments on $MgSiO_3$ are somewhat contradictory: the data for samples with $\rho_{00} = 2.76-3.04$ g cm^{-3}, which are located virtually on one $P(V)$ curve, lead to $\lambda \approx 0$, while the compressibility of samples with $\rho_{00} = 2.71$ g cm^{-3} implies that $\lambda < 0$. The $\lambda < 0$ property is also manifested by other silicates, in particular by tuff, which exhibits an anomalous mutual arrangement of Hugoniots with $\rho_{00} = 1.28$ g cm^{-3} and $\rho_{00} = 1.65$ g cm^{-3} for $P < 10$ GPa [9].

The behavior of the shock adiabats of fayalite and anorthite (see Fig. 13), which are initially in a low-density liquid state (at $T_0 = 1573$ K, $\rho_0 = 3.75$ g cm^{-3} and $T_0 = 1923$ K, $\rho_0 = 2.55$ g cm^{-3}, respectively), is qualitatively different from the behavior of similar shock Hugoniots for metals (see Section 5). In a significant part of the $P \leqslant 40$-GPa interval, these shock Hugoniots reside to the left of the principal shock Hugoniots which correspond to the initially dense solid material ($\lambda < 0$).

For relatively high pressures, the behavior of the shock Hugoniots depicted in Figs 10–13 exhibits a tendency to normalization ($\lambda > 0$).

One of the present authors (RFT) and his colleagues carried out experiments in the double shock compression of SiO_2 from the initial states with $P \approx 25$ GPa and $P \approx 35$ GPa, corresponding to the gently sloping portion of the shock Hugoniot with $\rho_0 = 2.65$ g cm^{-3} (the data have not been published). The resultant data in the (P, V) coordinates lie to the right of (are steeper than) the primary Hugoniot, while for metals (see Section 5) the opposite situation is observed. This feature may be attributed to the manifestation of the $\gamma < 0$ property by the substance. It is not unlikely that the same reason explains why the unloading isentropes of the silicates under consideration (α-SiO_2 [69, 70], fused silica [71], Mg_2SiO_4 [62], Fe_2SiO_4 [65], and $CaAl_2Si_2O_8$ [67]) lie to the left of the principal shock Hugoniots in approximately the same subdomain of (P, V) states where the shock wave $\lambda < 0$ property manifests itself. Qualitatively the same steep form is inherent in the isentropes of granite [72], rhyolite [73], and other silicates near the gently sloping portions of the principal shock Hugoniots. In paper[74], measurements were made of the wave profiles in the shock compression ($P \approx 10-20$ GPa) and the subsequent isentropic unloading of porous tuff with $\rho_{00} \approx 1.7-1.85$ g cm^{-3}. In gas dynamic calculations, the experimental data on the unloading could be reproduced only in the framework of the EOS model with $\gamma < 0$. Figure 14 gives the γ values in the states of shock compression employed in Ref. [74] to describe the experiment.

Therefore, experimental data with different silicates, including SiO_2 which has been studied most amply and constitutes their basis, testify to the realization, under shock compression, of the $\lambda < 0$ case and the steep secondary Hugoniots and unloading isentropes in a rather wide subdomain of states. This is qualitatively explicable in terms of $\gamma < 0$ property manifestation by the substance.

The realization of the situation with $\gamma < 0$ in SiO_2 in the intersection region of shock Hugoniots with different values of ρ_{00} was earlier noted in Ref. [75], and the possibility of explaining the steep SiO_2 isentropes was attributed to the manifestation of the $\gamma < 0$ property in Ref. [76].

Also noteworthy are several other peculiarities of the shock compression of silicates.

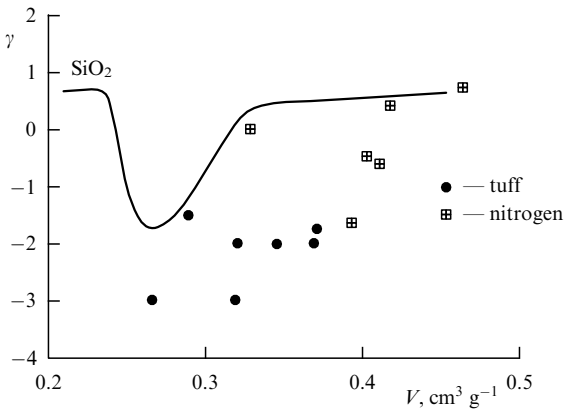

Figure 14. Behavior of the Grüneisen coefficient in shock-compressed states. Tuff [74] and nitrogen [92] data are shown by symbols; the solid curve represents calculations along the shock Hugoniot with $\rho_0 = 2.204$ g cm^{-3} in the framework of the SiO_2 EOS.

The shock Hugoniots depicted in Figs 10–13, in particular the Hugoniots corresponding to the close-to-maximal ρ_0 values (which have been studied in greatest detail), are, as a rule, nonmonotonic. For practically all silicates it is possible to mark out a gently sloping portion of the shock Hugoniot located in the $P \approx 10-40$ GPa range, as in the case with SiO_2 possessing $\rho_0 = 2.65$ g cm^{-3} (see Fig. 10). Here, the shock $P(V)$ dependences do not show clearly a sharp change of compressibility characteristic of the first-order phase transitions in the intersection of phase boundaries. In particular, the experimental shock Hugoniot of α-SiO_2 with $\rho_0 = 2.65$ g cm^{-3} in the case of realization of an equilibrium quartz–stishovite mixture would consist of three portions [79, 80] corresponding to α-SiO_2, the phase mixture, and the high-pressure phase — stishovite ($\rho_0 \approx 4.3$ g cm^{-3}). In this case, the second, gently sloping, portion of the curve corresponding to the phase mixture would reside in a very narrow pressure range $P_1 < P < P_1 + \Delta P$, $\Delta P \ll P_1$, where $P_1 \approx 6-9$ GPa — the onset pressure for the realization of the phase mixture (which somewhat varies, depending on the method of its estimation). The compressibility for this portion would be far greater than the compressibility in the first and third portions.

It is likely that the relatively smooth behavior of the Hugoniots observed in shock wave experiments is due to amorphization of the silicates at a high pressure (many of them, including SiO_2, Mg_2SiO_4, $MgSiO_3$, and $CaAl_2Si_2O_8$, transform into glass under shock and static pressures [79–85]) and to the peculiarities of the substance compression in this state. In particular, the existence of gently sloping portions of the silicate shock Hugoniots is attributed in Ref. [86] to the capacity of glass for enhanced continuous compaction in the pressure range corresponding to these portions. The smooth behavior of the fused-silica compression isotherm ($T = 300$ K) at pressures of up to $P \approx 60$ GPa (see Fig. 11) argues in favor of a continuous compaction mechanism.

Also possible for high values of parameters P, T is the decay (dissociation) of initial silicates to simpler components. Notably, the upper steep portions of the shock Hugoniots of continuous Mg_2SiO_4, $MgSiO_3$, and Fe_2SiO_4 samples are satisfactorily reproduced by models assuming the realization of $2MgO + SiO_2$, $MgO + SiO_2$, $2FeO + SiO_2$ mixtures and using for the oxides the EOSs characterizing their dense modifications (see, for instance, Refs [87–89]). In this case, a higher degree of decomposition of these components is supposedly not ruled out, either. The possibility was emphasized in report [90] that an $SiO_2 = SiO + 0.5O_2$ reaction may proceed under (P, T) conditions characteristic of the terrestrial mantle. In paper [91], an analysis was made of the structure of the material resulting from a spherical shock compression of a ball initially consisting of a mixture of α-SiO_2 and Al (the average initial mixture density $\rho_0 = 2.67$ g cm^{-3}). An analysis of intact samples in combination with gas dynamic simulation data showed that, judging by the presence of Si, Al_2O_3, and other substances in the final state, the initial α-SiO_2 begins to decompose in the solid state (prior to melting) with the release of oxygen on attaining a shock pressure of about 25–45 GPa (the former value corresponds to the highest pressure in the shock wave traveling to the ball center, and the latter value to the highest pressure in the secondary compression shock wave reflected from the center; the former shock wave passage time is significantly longer than the latter one). In this case, since the simplified EOS of the mixture employed in the gas dynamic simulations of Ref. [91] overrates the pressure in the $P \approx 25-60$ GPa range (by ≈ 30% in the middle of the range) in comparison with the experimental one, as well as due to the realization (see Ref. [91]) of higher temperatures in the shock compression of α-SiO_2 than in Al (at $P = \text{const}$), the decomposition of pure α-SiO_2 with $\rho_0 = 2.65$ g cm^{-3} supposedly commences at lower shock pressures than ≈ 25–45 GPa. When the substance state close to the point of decomposition initiation was approached, the authors of Ref. [91] recorded an increase in the amorphous quartz fraction (i.e. it is supposedly amorphous quartz which dissociates). No stishovite was detected in the intact samples. Clearly, the higher temperatures which characterize the shock compression of porous samples favor a lowering of the pressure at the point of SiO_2 dissociation onset.

In connection with the possibility of explaining the behavior of silicates by their decomposition in the shock compression, mention should be made of the qualitative similarity between the unusual properties manifested by the silicates and the features observed in the shock compression of dense nitrogen in the dissociation domain. Figure 15 depicts the experimental single-compression shock Hugoniot

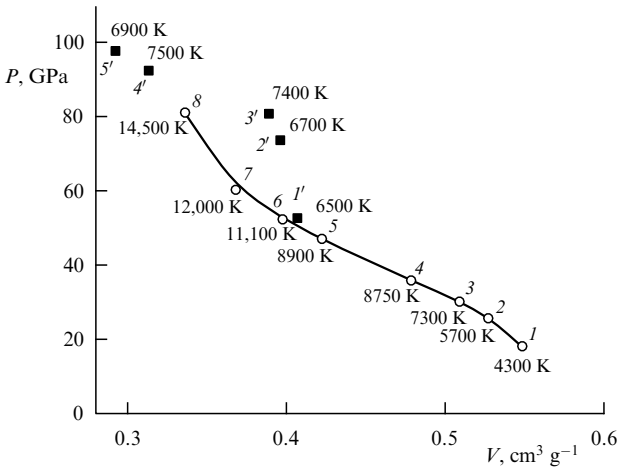

Figure 15. Experimental dependence (symbols) of the pressure in the single and double shock-wave compression of initially liquid nitrogen [92]. The solid curve stands for the single compression shock Hugoniot. *1–5* — initial states in the primary shock Hugoniot for double shock compression to the states *1′–5′*. Experimental values of temperature are indicated for states *1–8* and *1′–5′* [92].

of dense nitrogen corresponding to the initially liquid state with $T_0 \approx 77$ K, $\rho_0 \approx 0.808$ g cm^{-3}. This Hugoniot, like that of the silicates, possesses an intermediate gently sloping portion (for $P \approx 30-60$ GPa). According to Ref. [92], the $N_2 = 2N$ decomposition reaction proceeds in this pressure range. Figure 15 also shows the results of the double shock compression of nitrogen from the initial states *1–5*, which correspond to the primary shock Hugoniot, to the final states $1'-5'$. The states $1'-3'$ are located to the right of the single-compression shock Hugoniot. This is qualitatively consistent with the quartz steep secondary Hugoniots and the steep unloading of isentropes of silicates noted above, which may be attributed to the manifestation of the substance $\gamma < 0$ property. The realization of the $\gamma < 0$ situation in nitrogen is additionally confirmed by the data of temperature measurements [92] in states $1-8$ and $1'-5'$ (see Fig. 15). In states $1'-3'$, the values of V exceed the appropriate values in the primary shock Hugoniot (for equal pressures), while the values of T are lower in this case, resulting in the average $\beta < 0$ under these thermodynamic conditions (and, accordingly, to the average $\gamma < 0$ on the strength of formula (28)). The nitrogen average γ values calculated from shock compression data [92] are shown in Fig. 14. We note that the anomalous $\beta < 0$, $\gamma < 0$ values can be explained under the assumption that the volume v_{N_2} of one N_2 molecule is larger than the volume $2v_N$ of two N atoms produced in its decomposition. As a result, an increase in dissociation degree α with an increase in T leads (for instance, in isobars) to a lowering of the total mixture volume $(1-\alpha)\, v_{N_2} + \alpha(2v_n)$. The features in the behavior of nitrogen in shock waves are represented in Fig. 15 and appear evidently due to the properties of its EOS for a dense liquid-like state.

In view of the above arguments, it seems possible to provide a consistent qualitative explanation for the set of observed features in the behavior of silicates, which most likely manifest themselves in the amorphous state (with engagement of dissociation, judging by the data of Ref. [91]), in terms of the $\gamma < 0$, $\beta < 0$ properties inherent in the glass EOS in a rather broad subdomain of (P, T) parameters. In this case, the EOS thermodynamic functions remain relatively smooth, though not monotonic (the EOS of silicates is similar to that of liquid-like nitrogen). This interpretation is nonetheless hypothetical. Other approaches to the explanation of SiO_2 behavior are reviewed, inter alia, in Ref. [93]. The author of Ref. [93] (and some others) adhere to the viewpoint that the existence of gently sloping portions in the shock Hugoniots of α-SiO_2 with $\rho_0 = 2.65$ g cm^{-3} and fused silica with $\rho_0 = 2.204$ g cm^{-3} in the $P \approx 10-40$ GPa range and their anomalous mutual arrangement (intersection) for $P \approx 20-40$ GPa (see Fig. 10) are supposedly due to the thermally activated mechanism for the emergence of a high-pressure phase (crystalline stishovite) in a two-phase mixture of α-SiO_2 (a low-pressure phase) and stishovite with an increase in (E, T) parameters. Also discussed in Ref. [93] is the possibility of interpreting the behavior of the shock Hugoniots of initial α-SiO_2 and fused silica based on the approach employing a single-phase EOS of glass (the explanation of the specific features of quartz compression implied in the present paper). Pressures higher than $P \approx 20$ GPa are considered [under static ($T = 300$ K) compression, amorphization of initial α-SiO_2 begins at $P \approx 25$ GPa and comes to the end at $P \approx 30$ GPa [82]; as for shock compression, because of elevated temperatures which favor amorphization, the latter is expected to begin at lower pressures [93]]. According to Ref. [93], among the serious arguments against this interpretation may be the failure to explain the experimentally revealed intersection of initial α-SiO_2 and fused silica Hugoniots in the $P \approx 20$–40 GPa range, given the parameter $\gamma > 0$ for glass. However, a consistent explanation is provided for this feature under the assumption that glass exhibits the $\gamma < 0$ property. We note that measurements were made [94] of the structure (of the average coordination number) of fused silica in its static isothermal ($T = 300$ K) compression in the pressure interval $P \approx 0-100$ GPa. The experiments give evidence of a structural transformation in the $P \approx 20-35$ GPa range. Here, the authors of Ref. [94] are inclined to explain the resultant data in terms of the mechanism of continuous compaction of glass in a single-phase state (compressing like a one-component fluid) without realization of the mixture of low- and high-pressure phases. The data of other papers are also indicative of the continuous structural change of fused silica at high pressures along the $T = 300$ K isotherm. The compression isotherm of fused silica (see Fig. 11) obtained in Refs [55, 56] is, as noted above, also continuous, without sharp compressibility changes characteristic of the first-order phase transitions. These structure and compressibility data are at variance with the mix approach put forward by the author of Ref. [93]. With continuous compaction of fused silica along the $T = 300$ K isotherm, its continuous compaction is also probable under shock compression. The glass produced under the shock compression of α-SiO_2 with $\rho_0 = 2.65$ g cm^{-3} would also be expected to undergo continuous compaction.

The following remark is in order. As is seen from Fig. 11, the experimental $T = 300$ K fused-silica compression isotherm for $P \approx 20-40$ GPa lies above its shock Hugoniot. For the average temperature excess over a value of $T = 300$ K along the Hugoniot, this is attributable to the manifestation of the EOS $\gamma = V(\partial P/\partial T)_V/C_V < 0$ property, where $C_V > 0$ is the isochoric heat capacity. Therefore, both this feature and the intersection of crystalline- and fused-silica Hugoniots for $P \approx 20-40$ GPa may be due to the manifestation of the $\gamma < 0$ anomaly in the glass EOS.

As discussed in Section 2, significant variations in the dimension of initial SiO_2 particles for the same ρ_{00} value has no effect, to within experimental error, on the recorded shock wave velocity D (for the same external loading). The same result was yielded by check experiments on samples with the same ρ_{00} but different initial structures (crystalline or amorphous) [19, 75, 95]. Most likely, both of these results also argue against the realization, in shock-compressed states, of a phase mixture and the activation mechanism of the emergence of a high-pressure crystalline phase: for a diffusion production mechanism its amount would evidently depend on the initial material state, affecting the velocity D and the position of the shock Hugoniot. It is plausible to explain the independence of the final parameters from the initial ones by the transition of initially porous quartz to a vitreous state (amorphization which does not require surmounting activation barriers proceeds rapidly [93]) behind the shock front, and by melting at high temperatures. It is likely that the EOS of amorphous (glass and liquid) SiO_2 produced under shock compression from the initially porous substance also possesses the $\gamma < 0$ anomaly [which is a continuation of the $\gamma < 0$ anomaly, revealed from the shock Hugoniots of initially crystalline and fused silica in the interval $P \approx 20-40$ GPa to the domain of somewhat different (P, T) conditions], which is reflected in the unusual shape

of porous Hugoniots shown in Figs 10, 11. In connection with the assumption that $\gamma < 0$ states may be realized for a liquid, we note that a value of $\beta < 0$ is employed in describing the liquid phase for $P \approx 0-15$ GPa, $T \approx 2000-3200$ K in the multiphase EOS of SiO_2 [96].

Considering the qualitative similarity in the behavioral features of silicates and nitrogen in shock wave compression and their possible explanation in terms of dissociation, an attempt was undertaken in work [97] to describe on the basis of the mVdW model (see Section 4) the experimental data on the shock compression of fused and porous SiO_2 under the assumption of its decomposition at high pressures and temperatures into its SiO and O_2 components. According to the model used, it is assumed for initially porous silica that the silica in shock waves, irrespective of its initial (crystalline or amorphous) state, either becomes amorphous or passes to a liquid state. The model is defined by formulas (7)–(10), in which in the case under consideration $N_e = 0$, $i = SiO_2$, SiO, O_2, and $\sigma_i(T)$ is the internal statistical sum of an individual molecule. In the calculation of $\sigma_i(T)$, only the electronic ground state of the particles was taken into account; the molecular vibration and rotation were described by a rigid rotator–harmonic oscillator model [98]. The energies of SiO_2, SiO, and O_2 molecules in the ideal-gas state correspond to experimental values of dissociation energy. All molecular parameters were borrowed from reference book [99]. The mixture covolume $\bar{V}_C$ was taken to be additive relative to component covolumes: $\bar{V}_C(P^{rep}) = \sum_i N_i v_{C,i}(P^{rep})$ ($v_{C,i}$ is the covolume per particle). For an attraction pressure P^{att}, use was made of approximation (14) (independence of a detailed composition; in expression (14), $M = \sum_i m_i N_i$, and m_i is the mass of a molecule). The component covolumes and the attraction pressure were represented by simple functions containing free parameters. In the selection of SiO_2 covolume and attraction pressure parameters, we took into account the data on the isothermal ($T = 300$ K) compressibility of fused silica and its binding (sublimation) energy. The O_2 covolume was determined using data on the shock compressibility of liquid O_2. The covolume function of SiO was adjustable and was optimized for the best, so far as possible, model description of experiments on compressibility at high pressures. Equilibrium component concentrations were found from the equation $\mu_{SiO_2} = \mu_{SiO} + 0.5\mu_{O_2}$ with the application of detailed balance relations. At high T values, several other components (including ions and electrons) were also taken into account in the EOS [97], but their effect was found weak in the conditions considered below. In the execution of the calculations outlined below, the free covolume constants of the EOS were somewhat changed in comparison with their values in the version adopted in Ref. [97].

We emphasize that the EOS model under consideration is purely empirical in the domain of relatively high densities of substances (the model should be considered as a possible way of describing these experiments).

It is also pertinent to note that this model is close to the one employed in Ref. [100] for describing the properties of liquid and gaseous uranium dioxide (release of UO_2, UO, O_2 molecules and other similar particles, taking into account their 'sizes', modeling of statistical excitation sums by the statistical sums of ideal gas for all densities under consideration).

Figure 11 demonstrates the model shock Hugoniots of porous SiO_2 samples, as well as the shock Hugoniot and the $T = 300$ K isotherm of fused silica. In the calculation of shock compression, the strength effect, which is significant for fused silica for pressures $P < 20$ GPa, was disregarded (owing to the elevated temperatures reached under the shock compression of porous samples, on the whole one would expect a weaker manifestation of rheology effects along their shock Hugoniots than along the fused silica Hugoniot). In the solution of Eqn (3), E_{00} was taken to be equal to the calculated value for fused silica under normal conditions. As is seen from Fig. 11, the model provides a satisfactory description of the experiment on the isothermal and shock (for $P > 20$ GPa) compression of fused silica, as well as on the shock compression of porous samples. The model isotherm at $T = 300$ K, as in the experiment, passes above the model shock Hugoniot with $\rho_0 = 2.204$ g cm^{-3} in the $P \approx 20-40$ GPa range. Also reproduced is the fact that the values of V attained in the shock compression of samples with $\rho_{00} = 0.40-1.35$ g cm^{-3} are smaller than those realized in the isothermal ($T = 300$ K) compression of fused silica for $P \approx 5-20$ GPa (the calculated shock Hugoniots plotted in Fig. 11 intersect in approximately the same pressure range). The reproduction of these features is due to the existence of a subdomain of states in the EOS characterized by $\gamma < 0$. The calculated γ values along the shock Hugoniot with $\rho_0 = 2.204$ g cm^{-3} are shown in Fig. 14. The behavior of γ along other model Hugoniots depicted in Fig. 11 is qualitatively the same (with the γ minimum displaced towards higher V). The smooth dependences of γ also correspond to the smooth dependences of β (28). In the domain of $\gamma < 0$ property manifestation, the calculated shock Hugoniots of double compression and unloading isentropes are steeper than the principal shock Hugoniot. The negativity of model γ and β values is related to the fact that the total covolume of the $SiO + 0.5O_2$ mixture is smaller than the SiO_2 covolume (an analog of the $2v_N < v_{N_2}$ relation for nitrogen).

We believe that the results given in this section do not rule out the possibility that different silicates exhibit anomalous ($\gamma < 0$, $\beta < 0$) behavior in a vitreous state (its realization can be expected under compression with the possible engagement of the dissociation mechanism) in a rather broad (P, T, V)-parameter subdomain. As shown by the example with fused and initially porous SiO_2, reflecting this fact in the substance's EOS permits reproducing the main peculiarities of experiments at relatively high pressures.

7. Possible negativity of the Grüneisen coefficient in the upper terrestrial mantle

According to modern views, silicates like SiO_2, Mg_2SiO_4, $MgSiO_3$, and Fe_2SiO_4 may be the main rock-forming components of the mantle substance of Earth and other members of the terrestrial group of planets. One would expect that the physical characteristics of these silicates under the (P, T) conditions realized in the mantle would largely determine the properties (including the EOS) of the mantle substance; the possibility of realization of one process or another in the mantle (e.g. convection) depends on these properties. However, because the direct evidence is lacking, in particular data about the detailed composition and substance structure, much in abyssal geophysics remains hypothetical.

Since the main silicates can exhibit anomalous $\gamma < 0$, $\beta < 0$ properties (see Section 6), it seems expedient to briefly outline the hypothesis about the possible manifestation of this anomaly in the terrestrial mantle. These properties are supposedly inherent in the substance in a vitreous state,

which is apparently not ruled out for the mantle substance. Notably, according to Ref. [101] the upper part of the upper mantle resides in a crystalline state, and the lower part in an amorphous state.

The relatively smooth shock Hugoniots of silicates (see Figs 10–13) and the smooth isotherm at $T = 300$ K of fused silica (Fig. 11) also argue in favor of the realization of smooth distributions of different thermodynamic characteristics of the mantle with depth h, in particular the density $\rho(h)$ and the speed of sound $c_s(h)$. Such dependences take place in several terrestrial models constructed on the basis of seismological data and some other facts (since the recovery of mantle $\rho(h)$ and $c_s(h)$ distributions from seismological data is ambiguous, they may be represented either by continuous or discontinuous functions [102]). In what follows, we consider the case of continuous functions.

By way of example of a typical smooth distribution, Fig. 16 displays the $\rho(h)$ distribution for the B497 model borrowed from Ref. [103] (the author of this book, the well-known geophysicist K E Bullen, considered this model to be close to optimal). A salient feature of this distribution is a faster growth in ρ in the segment *1–2* (for $h \approx 200-1000$ km). Under the assumption of mantle substance uniformity, this can be explained in the following way. The density and pressure in the mantle are related as follows:

$$\frac{\mathrm{d}\rho}{\mathrm{d}P} = \left(\frac{\partial\rho}{\partial P}\right)_S + \left(\frac{\partial\rho}{\partial S}\right)_P \frac{\mathrm{d}S}{\mathrm{d}P}\,. \tag{30}$$

In view of the hydrostatic equation $\mathrm{d}P/\mathrm{d}h = \rho g$ (where $g(h)$ is the acceleration due to gravity) and the relation $(\partial\rho/\partial S)_P = -\gamma T\rho/c_s^2$, it follows from relation (30) that

$$\frac{\mathrm{d}\rho}{\mathrm{d}h} = \frac{\rho g}{c_s^2} - \frac{\gamma g T\rho^2}{c_s^2}\frac{\mathrm{d}S}{\mathrm{d}P}\,. \tag{31}$$

When $\mathrm{d}S/\mathrm{d}P = 0$ (i.e. the adiabaticity condition is fulfilled), the density distribution obeys the Adams–Williamson equation

$$\frac{\mathrm{d}\rho}{\mathrm{d}h} = \frac{\rho g}{c_s^2}\,. \tag{32}$$

Figure 16 depicts straight lines *1–1′* and *2–2′*, whose slopes $(\mathrm{d}\rho/\mathrm{d}h)_1$, $(\mathrm{d}\rho/\mathrm{d}h)_2$ were calculated proceeding from equation (32) (in these calculations and everywhere below it is assumed that $g = 9.9$ m s^{-2}) with the use of parameter values in states *1* and *2* defined by the B497 model: $\rho_1 = 3.38$ g cm^{-3}, $c_{s1}^2 = 41.2$ km^2 s^{-2}, $\rho_2 = 4.60$ g cm^{-3}, and $c_{s2}^2 = 76.1$ km^2 s^{-2}. In the steep *1–2* portion in Fig. 16, $\mathrm{d}\rho/\mathrm{d}h > \rho g/c_s^2$ everywhere (i.e. the density growth is superadiabatic), which is an indication that the second term on the right-hand side of expression (31) is positive: $\Delta_2 = -(\gamma g T\rho^2/c_s^2)\,\mathrm{d}S/\mathrm{d}P > 0$. This is possible when two conditions are met differentially and on average for $h \approx 200-1000$ km: $\gamma < 0$, and $\mathrm{d}S/\mathrm{d}P > 0$. The possibility of realizing the former condition is attested to by the characteristic features of the dynamic experiments on silicates discussed in Section 6. When $\gamma < 0$ and the mantle temperature $T(P)$ rises with an increase in P [in accordance with modern views (see, for instance, Refs [102, 104])], the latter condition, $\mathrm{d}S/\mathrm{d}P > 0$, is also fulfilled because

$$\frac{\mathrm{d}S}{\mathrm{d}P} = \frac{C_P}{T}\frac{\mathrm{d}T}{\mathrm{d}P} - \frac{C_P\gamma}{\rho c_s^2}\,. \tag{33}$$

As a result, for $\gamma < 0$ and $\mathrm{d}T/\mathrm{d}P > 0$ the complete condition $\Delta_2 > 0$ holds, which provides the enhanced (superadiabatic) growth of $\rho(h)$ dependence in the *1–2* portion in Fig. 16.

Substitution of expression (33) into expression (31) leads to the relation

$$\frac{\mathrm{d}\rho}{\mathrm{d}h} = \frac{\rho g}{c_s^2} - \frac{\gamma g C_P\rho^2}{c_s^2}\left(\frac{\mathrm{d}T}{\mathrm{d}P} - \frac{\gamma T}{\rho c_s^2}\right). \tag{34}$$

We estimate the average value of γ_m in the interval $h \approx 200-1000$ km using relation (34). For average values (marked with a subscript 'm'; $h_m \approx 600$ km), from relation (34) it is possible to obtain the following equation

$$\gamma_m^2 - \gamma_m\frac{\rho_m c_{sm}^2}{T_m}\left(\frac{\mathrm{d}T}{\mathrm{d}P}\right)_m - \left(\left(\frac{\mathrm{d}\rho}{\mathrm{d}h}\right)_m - \frac{\rho_m g}{c_{sm}^2}\right)\frac{(c_{sm}^2)^2}{\rho_m g (C_P)_m T_m} = 0\,. \tag{35}$$

Below, we use the following parameter values entering into equation (35): $(\mathrm{d}\rho/\mathrm{d}h)_m = 0.00153$ g cm^{-3} km^{-1}, $\rho_m = 3.99$ g cm^{-3}, $c_{sm}^2 = 58.7$ km^2 s^{-2} (calculated using linear relations for ρ and c_s^2 in the $h = 200-1000$ km interval and proceeding from the foregoing values of these characteristics in states *1* and *2*). It is assumed that $(C_P)_m = 3R/A$, where $R = 8.3\times10^{-3}$ kJ mol^{-1} K^{-1}, and $A = 20$ is the average atomic weight. The $T(P)$ dependence in the pressure range $P = P_1 - P_2$ (in the B497 model, states *1* and *2* in Fig. 16 correspond to $P_1 \approx 6$ GPa and $P_2 \approx 40$ GPa, respectively) was represented by the straight line

$$T = T_1 + T'(P - P_1)\,. \tag{36}$$

Parameters T_1 and T' were assigned as follows. In the computation of the $T(h)$ distribution in the mantle at a depth $h = 100$ km, it is usually assumed [102, 104] that $T \approx 1500$ K, ($\pm$ a few hundred degrees). In view of this, it is supposed that $T_1 = 1500$ K in formula (36) (possible variations of T_1 have only a minor effect on γ_m estimates). Two values were set for parameter T' in formula (36): 44.11 K GPa^{-1}, and 88.22 K GPa^{-1}. The former T' value corresponds to the temperatures $T_m = 2250$ K, $T_2 = 3000$ K calculated using

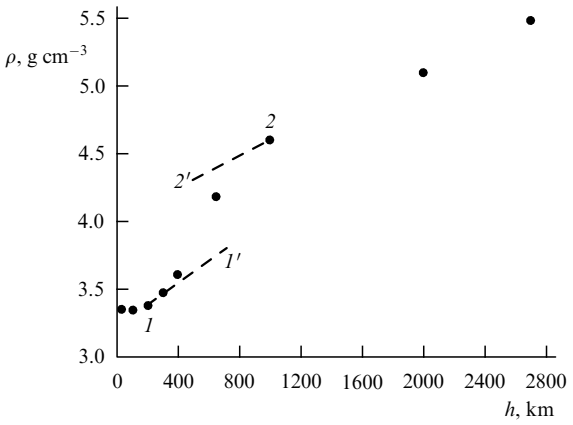

Figure 16. Density vs depth in the terrestrial mantle according to model B497 [103]. The slopes of straight lines *1–1′* and *2–2′* were calculated using the Adams–Williamson equation proceeding from the parameters in states *1* and *2*.

formula (36), and the latter corresponds to $T_m = 3000$ K, $T_2 = 4500$ K. To these, relatively low and high values of temperature T_c correspond at the mantle–core boundary (at $h \approx 2900$ km), equal respectively to ≈ 3500 K and ≈ 5000 K (these values are not at variance with T_c estimates [102, 104]). In the calculation of the T_c values on the basis of T_2 it was taken into account that the temperature increment in the lower mantle ($h \approx 1000-2900$ km) amounts to ≈ 500 K [102, 104]. This model estimate was obtained assuming an adiabatic temperature distribution in the lower mantle (determined from the condition $dS/dP = 0$). The validity of applying the adiabaticity condition is attested to by fulfillment to a high accuracy of the relation $d\rho/dh = \rho g/c_s^2$ in the $1000 \leqslant h \leqslant 2900$-km range for the B497 model version (see Fig. 16) and other mantle models. This leads to zeroing the second term on the right-hand side of expression (31), which requires fulfillment of the equality $dS/dP = 0$ when $\gamma > 0$ (the $\gamma > 0$ condition is assumed to hold true for $h > 1000$ km and $P > 40$ GPa). The most probable mechanism ensuring the approximate fulfillment of the adiabaticity condition comprises convection in the lower mantle. It is noteworthy that the relation $d\rho/dh = \rho g/c_s^2$ also holds in the outer terrestrial core, in which convection is commonly assumed to exist.

The employment of accepted parameters in equation (35) leads to the following values of the Grüneisen coefficient: $\gamma_m = -3.3$ for the former value of parameter T' in formula (36), and $\gamma_m = -2.2$ for the latter; these values are close in order of magnitude to the γ values for SiO_2 and tuff in the anomaly region (see Fig. 14). The resultant γ_m correspond to values of the expansion coefficient $\beta_m = \gamma_m (C_P)_m / c_{sm}^2$ equal to -7.0×10^{-5} K^{-1} and -4.7×10^{-5} K^{-1}, respectively.

Therefore, the superadiabatic growth in ρ in the *1–2* portion in Fig. 16 in the B497 model (and a similar feature in other smooth terrestrial mantle models) may be explained (for $dT/dP > 0$) by the manifestation of the $\gamma < 0$, $\beta < 0$ anomaly; this possibility is indicated by the data discussed in Section 6. It is noteworthy that the $\Delta_2 > 0$ condition stipulated in book [105] is a condition for the absence of convection in the medium.

8. Conclusions

Let us formulate the main results presented in this paper.

(1) A great body of data on the shock compression of initially porous metals has been accumulated over the 60-year-long period of research. This research has enabled penetrating into the domain of states of strongly heated (up to $T \sim 10^5$ K) and relatively low-density (with an expansion ratio of up to ≈ 5) liquid unattainable in other experiments. In the majority of cases, the experiments were carried out at pressures ranging up to ~ 100 GPa. For several metals (Fe, Cu, W, etc.), the peak pressures realized using the energy of nuclear explosions amounted to 1–2 TPa.

(2) An analysis, of the data on the shock compression of porous metals, supplemented with an analysis of experiments involving other methods (double shock compression, isentropic unloading, etc.), testify that metals possess conventional thermodynamic characteristics at high pressures and temperatures, and notably possess a positive Grüneisen coefficient.

(3) Experimental data on the shock compression of porous metals exhibited a significant decrease in the Grüneisen coefficient (by up to three times relative to its value under normal conditions) under the heating realized in the experiments, and thereby gave impetus to the development of new forms of wide-range EOSs model capable, in particular, of reflecting the properties of substances in a near-gaseous state.

(4) The wide-range EOS model reliant on the modified Van der Waals model reproduces the data of experiments in the shock compression of porous metals without special normalization to them. The data of other dynamic experiments are satisfactorily described as well. The model is helpful in estimating the EOSs of little-studied metals.

(5) Experiments at pressures ranging up to ~ 100 GPa on initially porous and low-density liquid samples of different silicates yield a result contradicting the metal compression law: in a significant pressure range, the density realized in their shock compression is higher than in the principal shock Hugoniot of initially dense materials. This anomaly may be qualitatively explained by the realization of substance states characterized by negative Grüneisen and thermal expansion coefficients. The silicates supposedly exhibit these properties in an amorphous form.

(6) The SiO_2 EOS constructed on the basis of the modified Van der Waals model with a negative Grüneisen coefficient in a rather wide subdomain of (P, T, V) parameters provides a satisfactory description of experimental data with fused and initially porous quartz.

(7) The negative value of the Grüneisen parameter may be the cause of superadiabatic (disobeying the Adams–Williamson equation) density growth in a major part of the upper terrestrial mantle.

Acknowledgments. The authors express their appreciation to V P Kopyshev for helpful discussions of several issues.

References

1. Al'tshuler L V *Usp. Fiz. Nauk* **85** 199 (1965) [*Sov. Phys. Usp.* **8** 52 (1965)]
2. Al'tshuler L V et al. *Zh. Prikl. Mekh. Tekh. Fiz.* (2) 3 (1981) [*J. Appl. Mech. Tech. Phys.* **22** 145 (1981)]
3. Avrorin E N et al. *Usp. Fiz. Nauk* **163** (5) 1 (1993) [*Phys. Usp.* **36** 337 (1993)]
4. Ahrens T J, Johnson M L, in *Mineral Physics & Crystallography: A Handbook of Physical Constants* Vol. 3 (Ed. T J Ahrens) (Washington, DC: American Geophysical Union, 1995)
5. Trunin R F *Usp. Fiz. Nauk* **164** 1215 (1994) [*Phys. Usp.* **37** 1123 (1994)]
6. Trunin R F *Usp. Fiz. Nauk* **171** 387 (2001) [*Phys. Usp.* **44** 371 (2001)]
7. Nellis W J *Rep. Prog. Phys.* **69** 1479 (2006)
8. Van Thiel M, Shaner J, Salinas E (Eds) *Compendium of Shock Wave Data* (Livermore, Calif.: Lawrence Livermore National Lab., 1977)
9. Marsh S P (Ed.) *LASL Shock Hugoniot Data* (Berkeley: Univ. of California Press, 1980)
10. Trunin R F (Ed.) *Eksperimental'nye Dannye po Udarno-Volnovomu Szhatiyu i Adiabaticheskomu Rasshireniyu Kondensirovannykh Veshchestv* (Experimental Data on the Shock-Wave Compression and Adiabatic Expansion of Condensed Substances) (Sarov: RFYaTs–VNIIEF, 2006)
11. Zel'dovich Ya B *Zh. Eksp. Teor. Fiz.* **32** 1577 (1957) [*Sov. Phys. JETP* **5** 1287 (1957)]
12. Zel'dovich Ya B, Raizer Yu P *Fizika Udarnykh Voln i Vysokotemperaturnykh Gidrodinamicheskikh Yavlenii* (Physics of Shock Waves and High-Temperature Hydrodynamic Phenomena) (Moscow: Fizmatgiz, 1963) [Translated into English (New York: Academic Press, 1966 – 1967)]
13. Al'tshuler L V, Krupnikov K K, Brazhnik M I *Zh. Eksp. Teor. Fiz.* **34** 886 (1958) [*Sov. Phys. JETP* **7** 614 (1958)]
14. Al'tshuler L V et al. *Usp. Fiz. Nauk* **166** 575 (1996) [*Phys. Usp.* **39** 539 (1996)]

15. Kormer S B et al. *Zh. Eksp. Teor. Fiz.* **42** 686 (1962) [*Sov. Phys. JETP* **15** 477 (1962)]
16. Trunin R F et al. *Zh. Eksp. Teor. Fiz.* **96** 1024 (1989) [*Sov. Phys. JETP* **69** 580 (1989)]
17. Trunin R F, Simakov G V *Zh. Eksp. Teor. Fiz.* **103** 2180 (1993) [*JETP* **76** 1090 (1993)]
18. Gryaznov V K et al. *Zh. Eksp. Teor. Fiz.* **114** 1242 (1998) [*JETP* **87** 678 (1998)]
19. Simakov G V, Trunin R F *Izv. Akad. Nauk SSSR Fiz. Zemli* (11) 72 (1991)
20. Trunin R F et al. *Zh. Eksp. Teor. Fiz.* **95** 631 (1989) [*Sov. Phys. JETP* **68** 356 (1989)]
21. Al'tshuler L V et al. *Zh. Eksp. Teor. Fiz.* **34** 874 (1958) [*Sov. Phys. JETP* **7** 606 (1958)]
22. Krupnikov K K, Brazhnik M I, Krupnikova V P *Zh. Eksp. Teor. Fiz.* **42** 675 (1962) [*Sov. Phys. JETP* **15** 470 (1962)]
23. Kopyshev V P, Medvedev A B, in *Vysokie Plotnosti Energii* (High Energy Densities) (Eds V N Mokhov et al.) (Sarov: RFYaTs–VNIIEF, 1997) p. 271
24. Kopyshev V P *Teoriya Uravnenii Sostoyaniya* (Theory of the Equations of State) (Sarov: FGUP RFYaTs–VNIIEF, 2009)
25. Sapozhnikov A T, Pershina A V *Vopr. Atom. Nauki Tekh. Metody Programmy Chislennogo Resheniya Zadach Mat. Fiz.* (4) 47 (1979)
26. Al'tshuler L V et al. *Zh. Eksp. Teor. Fiz.* **78** 741 (1980) [*Sov. Phys. JETP* **51** 373 (1980)]
27. Gordeev D G et al. *Vopr. Atom. Nauki Tekh. Teor. Prikl. Fiz.* (3) 19 (2010)
28. Bakanova A A, Dudoladov I P, Sutulov Yu N *Zh. Prikl. Mekh. Tekh. Fiz.* (2) 117 (1974) [*J. Appl. Mech. Tech. Phys.* **15** 241 (1974)]
29. Glushak B L et al. *Zh. Eksp. Teor. Fiz.* **96** 1301 (1989) [*Sov. Phys. JETP* **69** 739 (1989)]
30. Trunin R F, Simakov G V *Mat. Modelirovanie* **5** (8) 108 (1993)
31. Zhernokletov M V *Teplofiz. Vys. Temp.* **36** (2) 231 (1998) [*High Temp.* **36** 214 (1998)]
32. Funtikov A I *Teplofiz. Vys. Temp.* **36** 406 (1998) [*High Temp.* **36** 384 (1998)]
33. Trunin R F, Simakov G V, Medvedev A B *Teplofiz. Vys. Temp.* **37** 881 (1999) [*High Temp.* **37** 857 (1999)]
34. Gudarenko L F et al. *Teplofiz. Vys. Temp.* **38** 437 (2000) [*High Temp.* **38** 413 (2000)]
35. Trunin R F, Panov N V *Teplofiz. Vys. Temp.* **38** 754 (2000) [*High Temp.* **3**8 728 (2000)]
36. Trunin R F, Simakov G V, Panov N V *Teplofiz. Vys. Temp.* **39** 430 (2001) [*High Temp.* **39** 401 (2001)]
37. Zubarev V N et al., in *Doklady I-go Vsesoyuz. Simpoziuma po Impul'snym Davleniyam* (Proc. Ist All-Union Symp. on Pulsed Pressures), *Moscow, 24 – 26 October 1973* Vol. 1 (Moscow: VNIIFTRI, 1974) p. 61
38. Ragan C E (III) *Phys. Rev. A* **25** 3360 (1982)
39. Ragan C E (III) *Phys. Rev. A* **29** 1391 (1984)
40. De Beaumont P, Leygonie J, in *Proc. of the 5th Symp. on Detonation, Pasadena, 1970*, p. 430
41. Bushman A V, Fortov V E *Usp. Fiz. Nauk* **140** 177 (1983) [*Sov. Phys. Usp.* **26** 465 (1983)]
42. Kuropatenko V F, in *Vysokoskorostnoe Vzaimodeistvie Tel* (Fast Body Interaction) (Eds V M Fomin et al.) (Novosibirsk: Izd. SO RAN, 1999) p. 89
43. Val'ko V V et al., in *Fizika Yadernogo Vzryva* (The Physics of a Nuclear Explosion) Vol. 2 (Ed. V M Loborev et al.) (Moscow: Fizmatlit, 2010) p.140
44. Medvedev A B *Vopr. Atom. Nauki Tekh. Teor. Prikl. Fiz.* (1) 12 (1992)
45. Kopyshev V P, Medvedev A B *Sov. Tech. Rev. B Therm. Phys.* **5** (2) 37 (1993)
46. Kopyshev V P, Medvedev A B *Termodinamicheskaya Model' Szhimaemogo Kovolyuma* (Thermodynamic Model of Compressible Covolume) (Sarov: RFYaTs–VNIIEF, 1995) p. 58
47. Medvedev A B, in *Udarnye Volny i Ekstremal'nye Sostoyaniya Veshchestva* (Shock Waves and Extreme States of Matter) (Eds V E Fortov et al.) (Moscow: Nauka, 2000) p. 315
48. Medvedev A B *Fiz. Goreniya Vzryva* (4) 116 (2010)
49. Gryaznov V K, Iosilevskii I L, Fortov V E, in *Udarnye Volny i Ekstremal'nye Sostoyaniya Veshchestva* (Shock Waves and Extreme States of Matter) (Eds V E Fortov et al.) (Moscow: Nauka, 2000) p. 342
50. Gryaznov V K, Iosilevskii I L, Fortov V E *Pis'ma Zh. Tekh. Fiz.* **8** (22) 1378 (1982) [*Sov. Tech. Phys. Lett.* **8** 592 (1982)]
51. Trunin R F et al. *Teplofiz. Vys. Temp.* **33** (2) 222 (1995)
52. Duffy T S, Ahrens T J *J. Appl. Phys.* **76** 835 (1994)
53. Wackerle J *J. Appl. Phys.* **33** 922 (1962)
54. Knittle E, in *Mineral Physics & Crystallography: A Handbook of Physical Constants* Vol. 2 (Ed. T J Ahrens) (Washington, DC: American Geophysical Union, 1995)
55. Meade C, Jeanloz R *Phys. Rev. B* **35** 236 (1987)
56. Sato T, Funamori N *Phys. Rev. Lett.* **101** 255502 (2008)
57. Vildanov V G et al. *AIP Conf. Proc.* **370** 121 (1996)
58. Holmes N C, See E F, in *Shock Wave of Condensed Matter–1991* (Ed. S C Schmidt) (Amsterdam: Elsevier, 1992) p. 91
59. Holmes N C, in *High-Pressure Science and Technology–1993* (Ed. S C Schmidt) (Woodbury, N.Y.: American Institute of Physics, 1994) p. 153
60. Nikolaev D N et al. *AIP Conf. Proc.* **505** 121 (2000)
61. Trunin R F et al. *Zh. Eksp. Teor. Fiz.* **108** 851 (1995) [*JETP* **81** 464 (1995)]
62. Jackson I, Ahrens T J *J. Geophys. Res.* **84** 3039 (1979)
63. Ahrens T J, Lower J H, Lagus P L *J. Geophys. Res.* **76** 518 (1971)
64. Simakov G V, Trunin R F *Izv. Akad. Nauk SSSR Fiz. Zemli* (9) 80 (1973)
65. Chen G Q, Ahrens T J, Stolper E M *Phys. Earth Planet. Interiors* **134** 35 (2002)
66. Jeanloz R, Ahrens T J *Geophys. J. R. Astron. Soc.* **62** 529 (1980)
67. Boslough M B, Rigden S M, Ahrens T J *Geophys. J. R. Astron. Soc.* **84** 455 (1986)
68. Rigden S M, Ahrens T J, Stolper E M *J. Geophys. Res.* **94** 9508 (1989)
69. Podurets M A, Simakov G V, Trunin R F *Izv. Akad. Nauk SSSR Fiz. Zemli* (7) 3 (1976)
70. Chhabildas L C, in *Shock Waves in Condensed Matter–1985* (Ed. Y M Gupta) (New York: Plenum Press, 1986) p. 601
71. Chhabildas L C, Gray D E, in *Shock Waves in Condensed Matter–1983* Vol. 4 (Eds J R Asay, R A Graham, B V Straub) (Amsterdam: Elsevier, 1984) p. 175
72. Sekine T et al. *Geophys. J. Int.* **120** 247 (1995)
73. Anderson W W et al. *Geophys. J. Int.* **132** 1 (1998)
74. Erskine D, Nellis W J, Weir S T *J. Geophys. Res.* **99** 15529 (1994)
75. Trunin R F, Simakov G V, Podurets M A *Izv. Akad. Nauk SSSR Fiz. Zemli* (2) 33 (1971)
76. Swegle J W *J. Appl. Phys.* **68** 1563 (1990)
77. Davies G F *J. Geophys. Res.* **77** 4920 (1972)
78. Podurets M A, Trunin R F *Izv. Akad. Nauk SSSR Fiz. Zemli* (7) 21 (1974)
79. De Carli P S, Jamieson J C *J. Chem. Phys.* **31** 1675 (1959)
80. Jeanloz R et al. *Science* **197** 457 (1977)
81. Syono Y et al. *Science* **214** 177 (1981)
82. Hemley R J et al. *Nature* **334** 52 (1988)
83. Williams Q, Jeanloz R *Nature* **338** 413 (1989)
84. McNeil L E, Grimsdich M *Phys. Rev. Lett.* **68** 83 (1992)
85. Panero W R, Benedetti L R, Jeanloz R *J. Geophys. Res.* **108** 2015 (2003)
86. Stolper E D, Ahrens T J *Geoph. Res. Lett.* **14** 1231 (1987)
87. Al'tshuler L V, Trunin R F, Simakov G V *Izv. Akad. Nauk SSSR Fiz. Zemli* (10) 1 (1965)
88. Al'tshuler L V, Sharipdzhanov I I *Izv. Akad. Nauk SSSR Fiz. Zemli* (3) 11 (1971)
89. Telegin G S et al. *Izv. Akad. Nauk SSSR Fiz. Zemli* (5) 22 (1980)
90. Stishov S M, in *Khimiya Zemnoi Kory: Geokhim. Konf., Posvyashch. 100-letiyu so Dnya Rozhdeniya V I Vernadskogo, 14 – 19 Marta 1963. Tezisy Dokladov* (Chemistry of the Earth's Crust. Proc. of the Geochemical Conf. Commemorating the Centenary of Academician V.I. Vernadskii's Birth, 14–19 March, 1963) (Moscow: Izd. Akad. Nauk SSSR, 1963) p. 9 [Translated into English (Ed. A P Vinogradov) (Jerusalem: Israel Program for Scientific Translations, 1966)]
91. Kozlov E A et al. *Fiz. Met. Metalloved.* **104** 91 (2007) [*Phys. Met. Metallogr.* **104** 86 (2007)]
92. Nellis W J et al. *J. Chem. Phys.* **94** 2244 (1991)

93. Kuznetsov N M, in *Udarnye Volny i Ekstremal'nye Sostoyaniya Veshchestva* (Shock Waves and Extreme States of Matter) (Eds V E Fortov et al.) (Moscow: Nauka, 2000) p. 199
94. Sato T, Funamori N *Phys. Rev. B* **82** 184102 (2010)
95. Podurets M A et al. *Izv. Akad. Nauk SSSR Fiz. Zemli* (1) 16 (1981)
96. Swamy V et al. *J. Geophys. Res.* **99** 11787 (1994)
97. Zhernokletov M V et al. *AIP Conf. Proc.* **620** 763 (2002)
98. Landau L D, Lifshitz E M *Statisticheskaya Fizika* (Statistical Physics) (Moscow: Nauka, 1964) [Translated into English (Oxford: Pergamon Press, 1980)]
99. Glushko V P (Ed.) *Termodinamicheskie Svoistva Individual'nykh Veshchestv* Vols 1–4 (Moscow: Nauka, 1978–1982) [Translated into English: *Thermodynamic and Thermophysical Properties of Combustion Products* (Jerusalem: Israel Program for Scientific Translations, 1974)]
100. Gryaznov V K et al. *Izv. Ross. Akad. Nauk Ser. Fiz.* **63** 2258 (1999)
101. Kedrov O K *Seismicheskie Metody Kontrolya Yadernykh Ispytanii* (Seismic Methods for Monitoring Nuclear Tests) (Moscow: Inst. Fiziki Zemli RAN, 2005)
102. Magnitskii V A, Artyushkov E V, in *Tektonosfera Zemli* (Tectonosphere of the Earth) (Exec. Ed. V V Belousov) (Moscow: Nauka, 1978) p. 487
103. Bullen K E *The Earth's Density* (London: Chapman and Hall, 1975) [Translated into Russian (Moscow: Mir, 1978)]
104. Zharkov V N *Vnutrennee Stroenie Zemli i Planet* (Interior Structure of the Earth and Planets) (Moscow: Nauka, 1983) [Translated into English (Chur: Harwood Acad. Press, 1986)]
105. Landau L D, Lifshitz E M *Gidrodinamika* (Fluid Mechanics) (Moscow: Nauka, 1986) [Translated into English (Oxford: Pergamon Press, 1987)]